PLANT SCIENCES

Evolutionary metabolomics of specialized metabolism diversification in the genus *Nicotiana* highlights *N*-acylnornicotine innovations

David Elser[1], David Pflieger[1], Claire Villette[1], Baptiste Moegle[2], Laurence Miesch[2], Emmanuel Gaquerel[1]*

Specialized metabolite (SM) diversification is a core process to plants' adaptation to diverse ecological niches. Here, we implemented a computational mass spectrometry–based metabolomics approach to exploring SM diversification in tissues of 20 species covering *Nicotiana* phylogenetics sections. To markedly increase metabolite annotation, we created a large in silico fragmentation database, comprising >1 million structures, and scripts for connecting class prediction to consensus substructures. Together, the approach provides an unprecedented cartography of SM diversity and section-specific innovations in this genus. As a case study and in combination with nuclear magnetic resonance and mass spectrometry imaging, we explored the distribution of *N*-acylnornicotines, alkaloids predicted to be specific to *Repandae* allopolyploids, and revealed their prevalence in the genus, albeit at much lower magnitude, as well as a greater structural diversity than previously thought. Together, the data integration approaches provided here should act as a resource for future research in plant SM evolution.

INTRODUCTION

Plant metabolic profiles represent complex traits that reflect both evolutionary and temporally dynamic adaptations to specific ecological niches. Compared with their counterparts integrated into broadly conserved central C metabolism pathways, specialized metabolites (SMs) contribute to the largest fraction of intra- and interspecific variations in plant metabolic profiles. This plant chemodiversity is predicted to account for somewhere on the order of 100,000 to 1 million chemically unique structures, with an estimated range of 5000 to 15,000 structures per plant species (*1*). Many of these SMs act as chemical shields or as attractants in plant biotic interactions. In this respect, a relatively recent paradigm shift as part of ecological hypotheses such as the synergy (*2*) and interaction diversity hypotheses (*3*) has been to consider SM structural diversity, and not solely the summation of individual metabolites, as a critical determinant of plants' ecological interactions. The latter perspective also revives the interest in the exploration of SM diversity with modern analytical approaches and the use of adequate statistical descriptors (*4*).

In analogy to phylogenomics approaches that have flourished as a result of both the increasing release of annotated genomes and of established comparative bioinformatics pipelines to analyze these data, recent years have indeed seen a resurgence of plant family/genus–specific comparative metabolomics analyses to guide functional biochemical studies. For instance, comparative metabolomics within the Rhamnaceae revealed that only the Ziziphoid clade of this family has a functional triterpenoid biosynthetic pathway, whereas the Rhamnoid clade predominantly developed diversity in flavonoid glycosides (*5*). In a previous study, we implemented a metabolomics-centered fragmentation rule–based pipeline to annotate the diversity of 17-hydroxygeranyl linalool (17-HGL) diterpene glycosides within the Solanaceae family and revealed intense chemotypic structural variations combined with a patchy distribution of this compound class as it appeared restricted to the *Capsicum*, *Lycium*, and *Nicotiana* genera (*6*). The latter "phylometabolomics" information facilitated gene candidate selection for functional biochemical studies in the 17-HGL diterpene glycoside pathway (*6*). Similarly, comparative metabolomics across multiple Solanaceae species was instrumental in guiding coexpression studies for gene discovery for the steroidal glycoalkaloid pathway emblematic of the *Solanum* genus (*7*).

Besides interspecific variations in SMs, another important dimension, unfortunately rarely integrated into taxonomic-scale metabolomics studies, is the tissue/organ specialization of most SM pathways. Exploring these tissue/organ-level variations and their statistical correlation with gene expression data can be extremely powerful in the process of SM biosynthetic gene discovery (*8*). Analyzing tissue-specific metabolomes is also critical to test ecological theories of plant investments into metabolic defenses such as the optimal defense theory that predicts greater metabolic defense accumulation in developmental stages/tissues with higher organismic-level fitness contribution and/or greater predation rates (*9*). Trichomes, in particular glandular ones covering most aerial plant tissues, are notorious for their capacity to synthesize high amounts of very specific SMs (*10*). Trichome SMs can be either stored within trichome cells and glands or actively secreted, such as for Solanaceae-specific polyacylated sugars, also referred to as acylsugars and whose biochemistry has been thoroughly investigated in recent years (*11*). Calyces formed by the floral sepals and that protect maturating reproductive organs are typically rich in SMs whose biosynthesis can be dependent on trichomes present on these tissues (*12*–*14*). SM profiles of roots, while much less systematically explored than shoot-based ones, can be as structurally diverse as trichome-specific ones (*15*) and have recently become

[1]Institut de Biologie Moléculaire des Plantes du CNRS, Université de Strasbourg, Strasbourg, France. [2]Institut de Chimie du CNRS UMR 7177, Université de Strasbourg, Strasbourg, France.
*Corresponding author. Email: emmanuel.gaquerel@ibmp-cnrs.unistra.fr

of major focus for our understanding of SM ecological functions for plant-soil microorganisms' interactions (*16*).

Most recent advances in computational metabolomics provide a long-awaited framework to systematically explore the above-described importance of the species × tissue SM variations (*4*). These capacities to explore plant chemical spaces are further propelled by platforms such as, the MassIVE database (https://massive.ucsd.edu/) reaching 12,000 metabolomics datasets in 2022. Despite the increasing amount of data that can be generated from modern mass spectrometry (MS) instruments, the average annotation rate of most MS metabolomics studies remains at the order of a few percent of deconvoluted MS/MS features (*17*). The number of computational tools to address this challenge of transforming spectral information into chemical knowledge is hence rapidly increasing and can be divided into two main approaches. One set of approaches relies on MS/MS spectral grouping, as embodied by the game-changing development of molecular networking and of the repertoire of network annotation/mining tools embedded within the Global Natural Products Molecular Networking (GNPS) ecosystem (*18*, *19*). A second set of approaches relies on in silico fragmentation and (sub)structure prediction from mass spectra. Classification of spectra within ontologies of molecular families can notably be achieved by CANOPUS, a deep neural network method that is able to predict 2497 compound classes (*20*) and that is embedded with the elemental formula prediction and structure annotation pipeline from SIRIUS (*21*). Alternatively, the MS2LDA method allows the extraction of information derived from shared substructures from spectral data via a Latent Dirichlet Allocation algorithm borrowed from topic modeling (*22*). Recently developed or upgraded computational tools such as CFM-ID (*23*), molDiscovery (*24*), Metfrag (*25*), or QCxMS (*26*) (see the glossary of computational metabolomics tools presented as Supplementary Text) provide algorithmic means to predict MS/MS spectra from structures. However, systematically prioritizing and/or merging the highest confidence predictions from each of these tools remains a challenge that is rarely tackled in most MS metabolomic studies.

The genus *Nicotiana* L. combines several appealing features to study SM pathway diversification. This genus, comprising 13 well phylogenetically resolved sections for a total of at least 80 species, is appearing in various morphological forms such as small herbs to shrubs up to small trees, which often are viscid-glandular and rarely glabrous (*27*, *28*). Among the most studied species in this genus are *Nicotiana tabacum* and *Nicotiana rustica*, which are traditionally grown for tobacco products; *Nicotiana glauca*, which has been a focus of biofuel research studies (*29*); and *Nicotiana benthamiana*, a very popular model organism in molecular biology (*30*). The intense research on *Nicotiana* species is further reflected into the very large set of reference transcriptome and genome resources publicly available for species of this genus (*31*). As recently reviewed (*32*), the phytochemistry of several species of this genus, in particular that of the coyote tobacco *Nicotiana attenuata*, a flagship model organism for the chemical ecology of plant-insect interactions (*33*), has been extensively studied with notable focus on alkaloids, mono/sesquiterpene volatiles, acylsugars, or 17-HGL diterpene glycosides. Last, half of the species of the *Nicotiana* genus are allopolyploids of different ages, and, for some of them, the closest extant diploid progenitors have been mapped, thereby providing a phylogenetics framework to study allopolyploidy-mediated contributions to phenotypic trait evolution (*34*). Among the *Nicotiana* SM innovations thought to have been shaped by recent allopolyploidization events are *N*-acylnornicotines (NANNs), derived from the *N*-acylation of nornicotine with long-chain fatty acyl chains and which have been described as specific to allopolyploid species of the section *Repandae* (*35*). This *Nicotiana* section is about 4.5 million years old and has *Nicotiana sylvestris* as its closest diploid maternal and *Nicotiana obtusifolia* as closest paternal progenitor. The 17 NANN structures originally described in the *Repandae* species *Nicotiana repanda*, *Nicotiana nesophila*, and *Nicotiana stocktonii* (*36*, *37*), but not in *Nicotiana nudicaulis*, likely act as gain-of-function antiherbivory defenses. Compared with the *Nicotiana* widespread nicotine and nornicotine nonacylated alkaloids, NANNs are highly effective against and evade the resistance acquired for nicotine/nornicotine by the tobacco hornworm *Manduca sexta*, a native herbivore (*38*). However, the evolution of this defensive trait is largely underexplored, and detailed investigations on the NANN structural diversity within the genus *Nicotiana* are missing.

Here, we implemented a comprehensive computational MS metabolomics workflow to explore SM chemodiversity in various tissues of 20 species representative of the main phylogenetic sections within the *Nicotiana* genus. By using a multi-inference deep annotation approach that ultimately connects information theory statistics, chemical class mapping, and substructure inferences, we provide an unprecedented cartography of SM tissue-level distribution in this genus. The results of this study provide access to SM annotations and tissue × species distribution data to guide future biochemical studies and notably shed light on the unsuspected structural diversity and evolutionary trajectory of the NANNs defensive pathway within the *Nicotiana* genus.

RESULTS

Collecting tissue-level and phylogenetically relevant metabolomics data on *Nicotiana* SM diversity

To comprehensively explore tissue-level SM diversification in the *Nicotiana* genus, we profiled the metabolome of leaves elicited or not with methyl jasmonate (MeJA), concentrated leaf surface exudates, complete root and of calyces (Fig. 1B) of 20 species covering all of the main sections of this genus as well as diploid and allotetraploid states (Fig. 1A and table S1). Besides phylogenetic position, species selection further took into consideration the availability of transcriptomics/genomics data as a platform for future functional studies (*31*). Sampled tissues were selected on the basis of previous studies of our group (*8*), indicating the high degree of tissue-level specialization in SM distribution and, conversely, the importance of concatenating multitissue profiles to increase SM coverage. In addition, we aimed via this pluri-tissue approach to exploring tissue-level shifts in SM class prevalence across the focal species as a mechanism of organismic-level chemodiversification. Noteworthy, amounts of leaf exudate material collected greatly differed among the focal species, with *Nicotiana setchellii* (2.7 mg of exudate per g of leaf fresh weight) and *Nicotiana glutinosa* (2.5 mg/g) producing the largest amounts of dried exudates collected from leaf washes (fig. S1 and table S1). All methanolic extracts were analyzed using a previously established UPLC-ESI$^+$-QTOF MS (ultraperformance liquid chromatography-positive mode electrospray ionization quadrupole time-of-flight MS) method with optimized settings

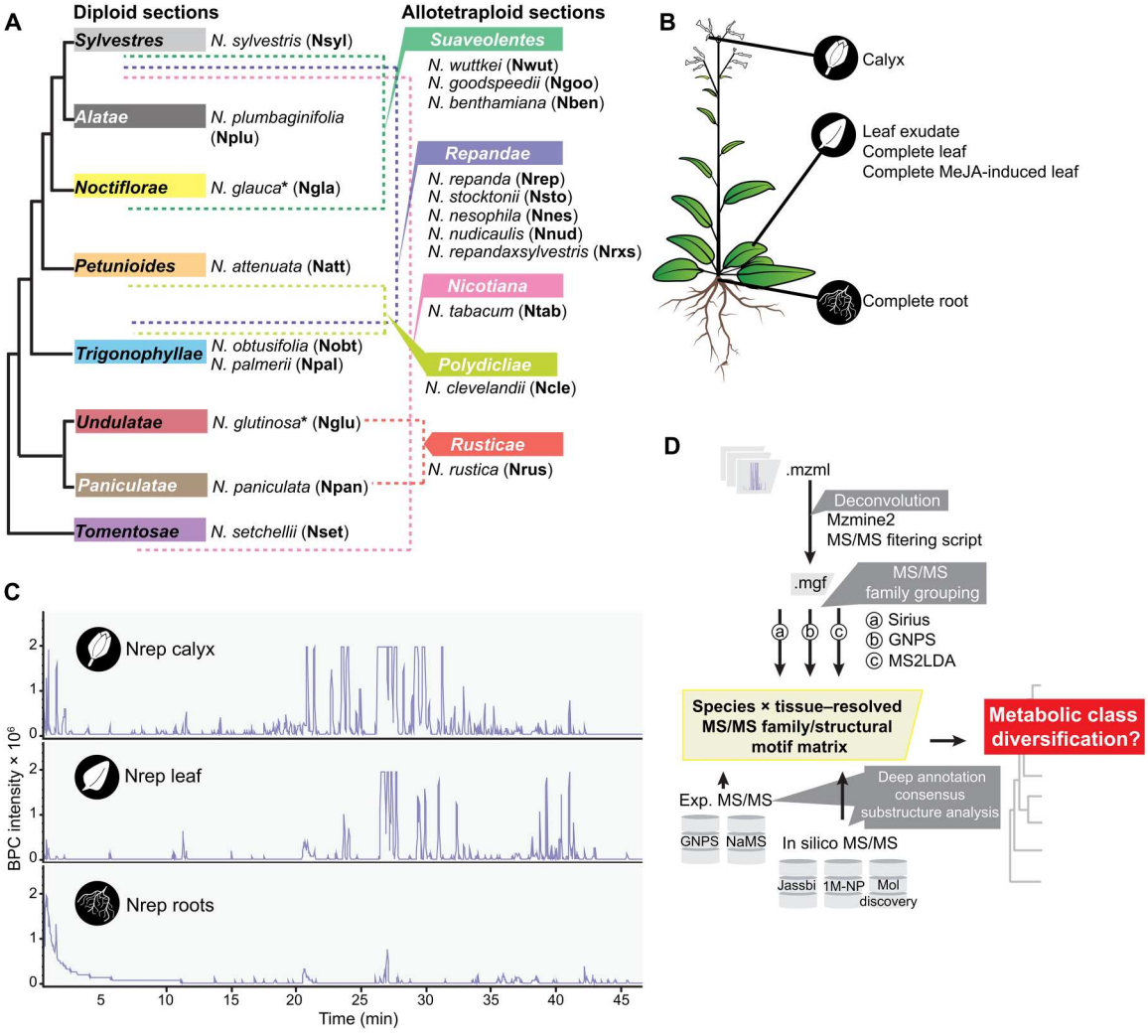

Fig. 1. Experimental and data processing setups to explore species × tissue–specialized metabolism diversification in the *Nicotiana* genus. (**A**) Schematic *Nicotiana* phylogenetic tree highlighting main genus sections and representative species selected for metabolomics analysis. Four allotetraploid sections, dashed lines indicate sections containing closest extant diploid progenitors. Accessions and origins of the selected species are referred to in table S1. *N. glutinosa** and *N. glauca** are considered as homoploid hybrids as summarized in (*34*). (**B**) Tissue sampled from 6 to 8-week-old plants of the selected 20 *Nicotiana* species. Fully elongated leaves were considered for leaf-based samplings. Leaf exudates were prepared by acetonitrile-based leaf surface rinsing; MeJA-treated leaves were harvested 72 hours after treatment. (**C**) Representative base peak chromatograms (BPCs) from the UPLC-ESI$^+$-QTOF MS analysis of methanolic extracts of *N. repanda* roots, untreated leaves, and calyces. (**D**) Data processing pipeline to construct a species × tissue MS/MS spectral matrix and for its deep structural annotation before metabolic class diversification analysis. Architecture of the data processing pipeline and organization of the different output matrices as supplementary datasets are presented in fig. S2.

for massive MS/MS data collection (*6*). A total of 17,901 metabolite-derived MS/MS spectra (hereafter referred to as features) were, after a data redundancy and contaminant check using a custom script, deconvoluted and considered for feature-based molecular networking (FBMN) processing with settings that were optimized to handle the species × tissue–exacerbated metabolic diversity in the dataset. The resulting species × tissue MS/MS feature compendium served as input for the data exploration workflow presented in Fig. 1D (fig. S2).

To contrast patterns of feature diversity across species, we calculated, for each of the tissue types, α-diversity scores based on the Shannon entropy (H) from information theory (*8*) (Fig. 2A). A unifying trend in these tissue-level analyses was that species′ profiles, differed extremely in their α-diversity indices, up to threefold counterspecies variations being detected depending on the tissue type. Root samples were, from all examined plant samples, those with consistently lower α-diversity scores (average H = 7.6), likely indicative of the prevalence of only a few SM classes in these samples for the analytical conditions considered in this study (Fig. 1C). As expected, highest α-diversity scores were, on average, detected for MeJA-elicited leaves (average H = 9.4) (fig. S3), followed by uninduced leaves (average H = 9.3) and calyces (average H = 9.0). The effect of the MeJA elicitation on feature diversity was consistently more apparent at the level of detected features and very variable among the focal species (fig. S3). We noted that these interspecies variations in MeJA inducibility (indicative of the amplitude of a "metabolome plasticity" to this treatment) were strongly negatively correlated (Pearson correlation coefficient = −0.76, P =

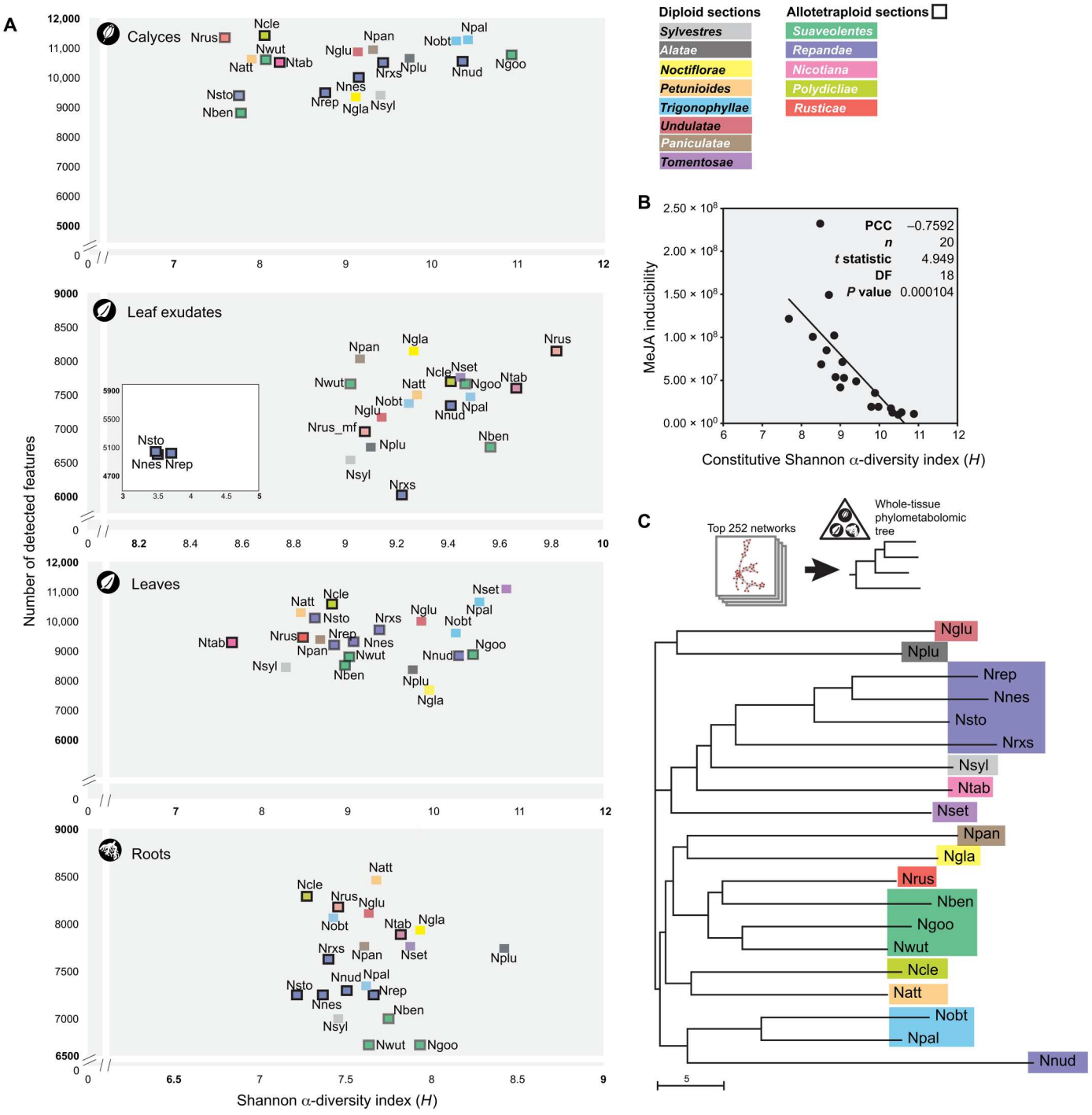

Fig. 2. Species metabolome α-diversity and phylometabolomics relatedness. (**A**) Biplots depict the number of detected features and the information theory Shannon α-diversity as an index of feature richness per tissue. *Nicotiana* phylogenetic sections are color-coded, and squares with black strokes are used for allopoplyploid species. (**B**) Biplot visualizing the interspecies negative correlation between leaf metabolome MeJA inducibility (calculated from the Euclidean distance between MeJA-induced and uninduced leaf profiles) and constitutive (uninduced leaf samples) α-diversity. PCC, Pearson correlation coefficient; DF, degree of freedom. (**C**) Phylometabolomics tree computed from the molecular networking information. To analyze the relatedness of species' metabolomes, we first computed interspecies Euclidean distances based on the molecular networking information and used the resulting distance matrices for constructing a phylometabolomics tree based on the neighbor-joining algorithm (bootstrap values derived from 999 iterations) (table S2). Trees were also constructed from the tissue-level data (fig. S4).

1.04×10^{-4}) with α-diversity scores of uninduced leaves ("constitutive diversity") (Fig. 2B). In addition, while we initially assumed that the metabolic profiles of the exudates collected from uninduced leaves would be restricted to a few prevalent SMs (thereby resulting into in low α-diversity scores for this sample type), the relatively high α-diversity scores detected in most species were consistent with a far greater chemical diversity in those extracts. In clear contrast, *Repandae* species, with the exception of *N. nudicaulis* and the hybrid *N. sylvestris* × *N. repanda*, exhibited much lower α-diversity scores (*H* ranging from 3.5 to 3.7 compared with the average *H* value of 8.5 for the rest of the species) that were in line with the previously reported overdominance of NANNs within their exudates (*37*). When feasible based on the species sampling, we also compared the α-diversity scores of allotetraploid species to those of closest diploid progenitors. Independently of the tissue type considered, we did not observe a tendency for higher α-diversity scores in allopolyploids as compared to those of closest diploid progenitors (Fig. 2A).

To analyze the relatedness of species' metabolomes, we further computed interspecies metabolic distances based the molecular networking information and used the resulting distance matrices for constructing phylometabolomics trees. Several studies had previously attempted to construct such phylometabolomics trees but from single-tissue metabolome data. Here, we constructed trees both from the tissue-level (fig. S4) and combined tissue data (Fig. 2C). The resulting "all tissues" phylometabolomics tree captured patterns of metabolome relatedness that were frequently in accordance with the species' tree section-level grouping and relatedness (Fig. 2C). Among other interesting insights, *Repandae* species' metabolomes, with the exception of that of *N. nudicaulis*, appeared much closely related at the all tissues metabolome level to that of the *Sylvestres* section from which their maternal progenitor had been associated with than to the *Trigonophyllae* section (paternal progenitor section) (Fig. 2C and table S2). This analysis could not be transposed for *N. tabacum* and *N. rustica* allopolyploids for which one of the closest diploid progenitors had unfortunately not been initially included in the species selection.

Creating a cartography of *Nicotiana* SM class diversification

After highlighting counterspecies chemodiversity variations, we then systematically characterized onto which SM classes they mapped. In analogy to gene family inference and survey across focal species as a first step in phylogenomics, we first used the CANOPUS tool for ad hoc systematic compound class and chemical ontology predictions. To combine FBMN and CANOPUS information, we implemented a frequency-based molecular network–based propagation of CANOPUS (NP-CANOPUS) predictions, resulting into class predictions for 86.5% of the total features within the 1586 networks retrieved by FBMN. CANOPUS "superclass" and "most specific class" intensity distributions integrating all tissue samples of given species were encapsulated as treemaps and mapped onto the species tree to provide a bird's eye view on class expansions and shrinkages (Fig. 3B). For the sake of simplicity, only a few of the main tendencies are reported below; close-up views on particular "metabolic tiles" and tissue-specific treemaps are accessible in data S1. Most clearly apparent was the highest proportion of "lipids and lipid-like molecules" in all species, with a substantial fraction of these lipids being, in many species, contributed by the saccharolipid subclass commonly referred to as acylsugars in the Solanaceae. Browsing these treemaps supported the presence of high amounts of predicted diterpenes in *N. tabacum*, *N. sylvestris*, and the cross between *N. repanda* × *N. sylvestris*—the latter hybrid having been initially incorporated to test progenitor chemical trait dominance. Among other trends, this analysis also pinpointed on *N. setchellii* exhibiting the most diverse and abundant set of "phenylpropanoid derivatives" from predicted 3-*O*-methylated flavonoids (connected to network #361), simple hydroxycinnamic acids (network #990), up to coumarin glycosides (network #532). Noteworthy, the performance of CANOPUS predictions was nonetheless hampered for SMs that contained substructures from independent biosynthetic origins, thereby resulting into heterogeneous CANOPUS ontologies. For instance, the large "amino acids and derivatives" tile within the *N. glauca* treemap was mostly associated with network #468, but the features embedded in this network were manually curated as *N*-hydroxycinnamoyl-spermidine conjugates that are commonly encountered in leaves of Solanaceae species as antiherbivore defenses (*39*). This limitation was also highlighted by the fact that the high level of NANNs, which are emblematic of the *Repandae* section, was not as easily noticeable on the corresponding treemaps. Previously characterized NANNs were indeed split into several classes as "organoheterocyclic compounds," "benzenoids," and "organic nitrogen compounds" (data S1).

Deep metabolome annotation empowered by a multi-inference approach incorporating a 1 million natural product in silico spectral database and consensus substructure computations

The previous analysis indicated a critical need not only for broadly increasing feature annotations beyond CANOPUS class predictions but also for gaining structural insights into core (sub)structures underlying molecular networks' topology. As outlined in a recent review (*40*), substructure annotation provides information about functional groups, building blocks, or scaffolds within a chemical structure. This level of information is complementary to compound class prediction, most commonly addressing biosynthetic origin and/or compound physicochemical properties. To propel substructure identification in our dataset, we first optimized a multi-inference annotation pipeline (figs. S2 and S5). Briefly, feature spectra were first queried against an in-house *Nicotiana attenuata* SM MS/MS database (entries resulting from the analysis of purified SMs) and the GNPS library, the resulting hits being referred respectively to as annotation levels 1 to 2 according to the Metabolomics Standard Initiative nomenclature (*41*). Interrogation of these two experimental spectral databases provided hits for 4% of the MS/MS features (Fig. 3A). Level 3 of the annotation nomenclature regrouped class-based annotations mostly derived from manual inspection of network-level hits (5%). To circumvent limitations in the chemical space covered by these two experimental databases, we conducted spectral interrogations in parallel against in silico predicted MS/MS spectral libraries using both molDiscovery that predicts MS spectra of small molecules on the fly and scores their probabilistic modeling (*24*) and a combination of CFM-ID and MatchMS. To further expand the power of this approach beyond the chemical space of the molDiscovery built-in library, we computed MS/MS spectra for the 429 natural products reported in a recent *Nicotiana* phytochemistry review (*32*) and undertook the development of an in silico spectral library for about 1.1 million natural products (1M-NP, hereafter referred to as 1M-DB).

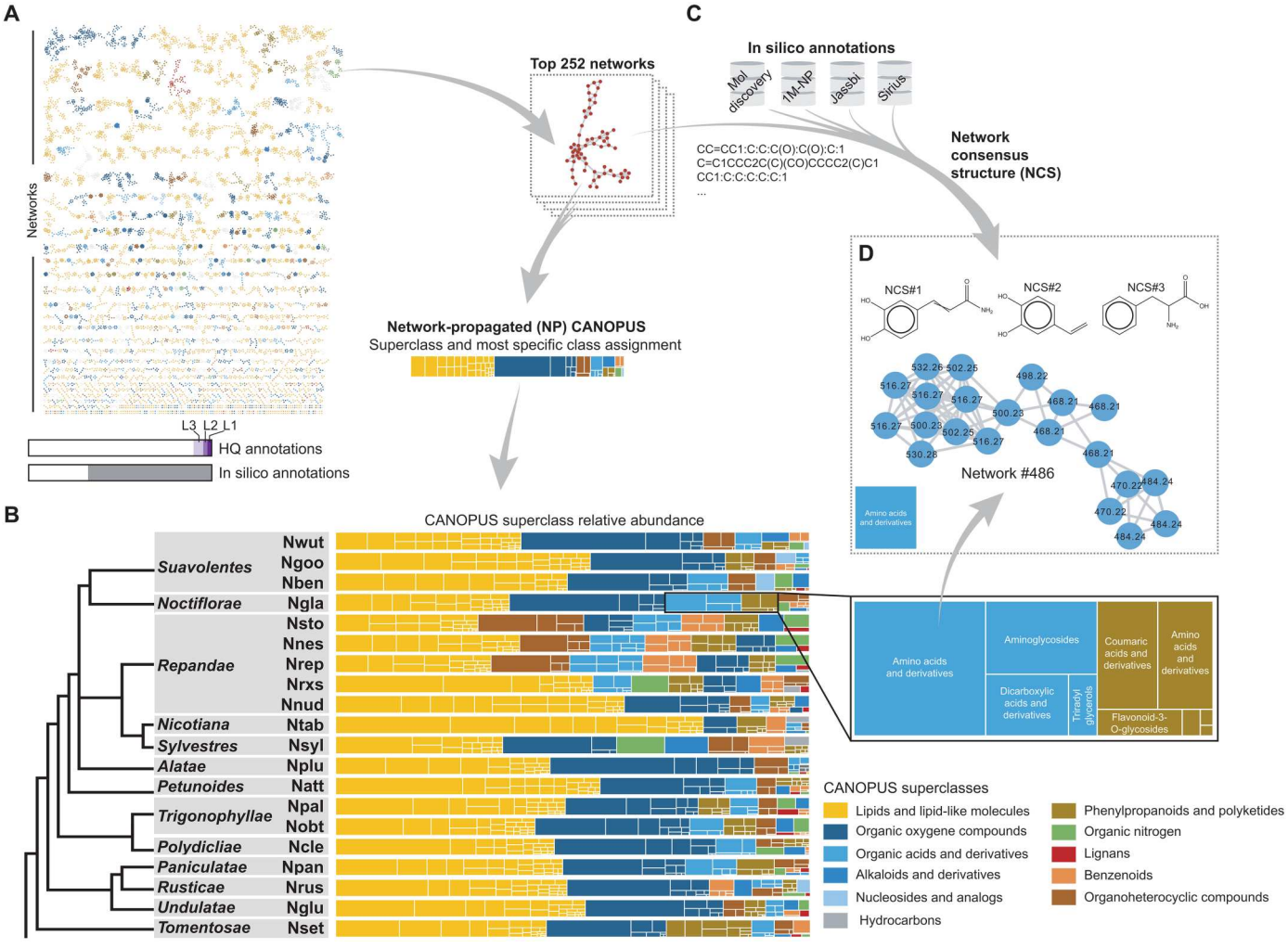

Fig. 3. Cartography of *Nicotiana* species–level metabolic class and substructure distribution using a molecular network–propagated consensus substructure approach. (**A**) Molecular networking of species × tissue–deconvoluted MS/MS features. The top 252 molecular networks were retrieved for a minimum MS/MS pairwise cosine value of 0.7 and of six matching mass/charge ratio (*m/z*) signals. Node colors refer to network-propagated CANOPUS superclass predictions. Bars refer to the relative proportions of individual MS/MS further annotated from the three levels of annotation confidence (see Materials and Methods) or with databases build from in silico generated MS/MS spectra [see (C)]. HQ, high quality. (**B**) Treemap visualization of species-level superclass and most specific class distribution. Colors denote for different NP-CANOPUS superclasses, with each individual uniformly colored rectangles depicting most specific classes hierarchically classified as part of a NP-CANOPUS superclass. A close-up view on two superclasses ("organic acids and derivatives"/"phenylpropanoids and polyketides") detected in *N. glauca* (Ngla) is presented. (**C**) Network consensus structure (NCS) computations from hits obtained from the interrogation of in silico generated MS/MS spectra (fig. S10). Hits obtained for each MS/MS feature–level database search within a network were compiled input to compute a consensus (sub)structure for each network. (**D**) NCS computed for network #486 whose MS/MS features were classified in (A) as those of amino acids and derivatives. The library of feature/network/NP-CANOPUS/NCS associations is reported in data S1, S3, and S4.

A comprehensive description of the creation of the 1M-DB in silico spectral library and of its architecture is reported in Supplementary Text (see also figs. S6 and S7). The capacity of such in silico spectrum–based approach to increasing the annotation coverage of plant SM profiles has initially been exemplified in a pioneer study by Allard *et al.* (*42*) but was restricted to chemical entries (~220,000) retrieved from the copyrighted Dictionary of Natural Products (http://dnp.chemnetbase.com). Here, we concatenated chemical structures derived from several public natural product libraries (table S3), which resulted, after filtering out duplicated InChI representations and CFM-ID–based computation of composite MS/MS spectral predictions, into 1,066,512 unique MS/MS spectra that covered a vast proportion of the natural product chemical classification proposed by NPClassifier (*43*). As CFM-ID version 4.0 computations returned slightly different MS/MS spectra for enantiomers [see MS/MS spectra predicted (+)−/(−)-shikonin and (+)−/(−)-thalidomide in fig. S8), stereoisomers (enantiomers and diastereoisomers) were kept in the library. Together, this important computational delivery of this study represents, to the best of our knowledge, the largest natural product–derived in silico spectral library and is now available for spectral interrogation as part of the GNPS ecosystem (see Data and Material Availability).

The above-described multiquery approach of the 17,901 features from our dataset retrieved annotations for 57% of these features, with 9% hits for priority levels 1 to 3 (Fig. 3A). To maximize structural insights that could be gained from this deep annotation, we lastly computed the top most common substructures [referred to as network consensus structure (NCS)] based on feature annotations for each of the FBMN molecular networks that did not contain any level 1 to 2 annotations. Consensus structure computational prediction relies on an algorithmic approach that uses hits obtained from in silico MS/MS spectral databases (see description in Materials and Methods and "Code availability" section). The NCS strategy is illustrated in Fig. 3 (C and D) with top NCS hits for network #486 whose MS/MS features were initially classified as amino acids and derivatives by CANOPUS. A complete overview of the top NCS predictions is summarized in data S3. Together, this unique combination of different computational approaches generated a multimodal SM cartography that can be navigated from CANOPUS-based ontology predictions down to sets of molecular networks connected to a given class level and further down to predicted shared substructures within these networks (data S3 and S4).

Exploring the chemical substructure basis of *Nicotiana* section and species-level SM specialization

Next, we navigated the SM cartography to further dig into the interspecies chemodiversity variations that were detected from the species-level α-diversity (Fig. 2) and CANOPUS treemap analyses (Fig. 3). To rigorously infer statistical associations between species and particular CANOPUS superclass/most specific class predictions, we used nonmetric multidimensional scaling (NMDS). NMDS is a powerful ordination technique in information visualization that is frequently used in ecology to spatially represent interconnections among species or communities based on a series of univariate descriptors (*44*). The strength of this statistical approach is that it allows to efficiently collapse the information from multiple dimensions (here summed peak areas and connected CANOPUS predictions) into a limited number of descriptors exhibiting high-confidence statistical associations to species. Using NMDS, we computed projections of species and CANOPUS predictions as intrinsic variables and extracted strongest associations based on $P < 0.05$ (permutation tests) and minimal cosine scores for angular distances between these two set of entities in NMDS projections (Fig. 4A and data S2). A hierarchical clustering analysis of previously extracted most significant associations resulted into four main clusters referred to as family clusters (FCs) (Fig. 4B). Distribution of these associations was not directly consistent with the species/section phylogeny and thereby indicative of gains and losses in species/section-level capacities for the abundant production of specific SM core structures. FC1 regrouped predictions associated to *O*-acylglycerol structures that appeared to be prevalent within species of the section *Suaveolentes* and, to a lower extent, in the *Petunoides*, *Polydicliae*, *Paniculatae*, and *Rusticae*. In accordance with the pronounced expansion of this compound class in the *Nicotiana* genus (*11*), acylsugar predictions enriched in FC2 exhibited widely distributed significant species associations throughout the genus. These associations were remarkably absent for the section *Repandae*, with the exception of *N. nudicaulis*. Strong associations with predicted terpenoid structures caught our attention when inspecting FC3. Most distinctive ones were detected for sections *Nicotiana* and *Sylvestres* as well as for more distantly related sections *Undulatae* and *Tomentosae*. FC4 mostly captured associations with phenylpropanoid-derived substructures and alkaloids, the latter further emphasizing on the richness of alkaloid metabolism in the *Repandae* section.

A detailed interpretation of these species/section metabolic specificities requires a simplified access to the underlying MS/MS fragmentation schemes. The latter can typically be approached through MS2LDA, an unsupervised method to extract common patterns of mass fragments and neutral losses, referred to as mass motifs, from collections of fragmentation spectra (*22*). From this analysis, we retained 76 mass motifs that best depicted the structural diversity within our dataset as confirmed by hierarchical clustering (resulting in clusters of covarying mass motifs) and mapping of enriched CANOPUS predictions for each mass motifs (motif-level propagation of CANOPUS predictions) (Fig. 5A and fig. S9). In analogy to the critical role of conserved domain/motif inferences in protein structure-activity studies, mass motif inference offers a dimensionality reduction perspective on recurrent fragmentation patterns derived from particular substructures. This approach is, however, often limited by the scarcity of structurally annotated mass motifs in MS2LDA libraries. An asset of our approach is that it mutualizes the previously described SM cartography to mine most interesting mass motifs (Fig. 5B and data S5). As a proof of function of our approach, we notably confirmed the presence in motif cluster 1 (MC1) of a mass motif (Strepsalini_110) that was characteristic of the *O*-acylglycerols specific to *Suaveolentes*. MC1 also contained motif #631 and motif #254 characteristic of steroidal glycoalkaloids that were notably specific to *Nicotiana plumbaginifolia*. Motif #646, present in the second cluster (MC2), captured the complete diversity of 17-HGL diterpene glycosides, allowing to efficiently explore the tissue specificity for this compound class. MC4 contained a motif (motif #37) with fragments indicative of hydroxycinnamic acid substructures derived from a network of *O*-phenolic glycosides. Similarly, by using inferences derived from these different computational approaches, we could also efficiently inspect motifs corresponding to additional case studies such as *N*-hydroxycinnamoylspermidine conjugates specific to *N. glauca* (MC5, motif #473); di- and triterpenoids abundantly found in *N. tabacum* (MC5, e.g., motif #555 and #euphorbia_350); and mono-, sesqui-, and diterpenes (MC5, motifs #558, #675, and #576, respectively) in sections *Nicotiana* and *Sylvestres* as well as *Undulatae* (fig. S10). As previously implemented for molecular networks (Fig. 3), mass motifs can also be used for consensus substructure computations [motif consensus structure (MCS)], the latter providing a further mean to circumvent the scarcity mass motif annotation in MS2LDA libraries. All 76 MCS computations, combined with CANOPUS predictions and manual curation, are presented in data S6. Last, we provide, using the diversification of leaf surface acylated sugars/glycerols as a case study, a step-by-step illustration of how biological insights could be gained from such an integration of molecular network and substructure information–derived mass motifs, MCS and NCS computations. To this end, three CANOPUS class predictions, that of "alkyl glycosides," "1-monoacylglycerols," and "saccharolipids," which are broadly connected with acylated sugars/glycerols, were queried for their species-level associations as well as corresponding MCS and NCS computations (Fig. 6A). Figure 6B provides a closer perspective into the CANOPUS prediction for alkyl glycosides (network #372 and mass motif #586), corresponding to

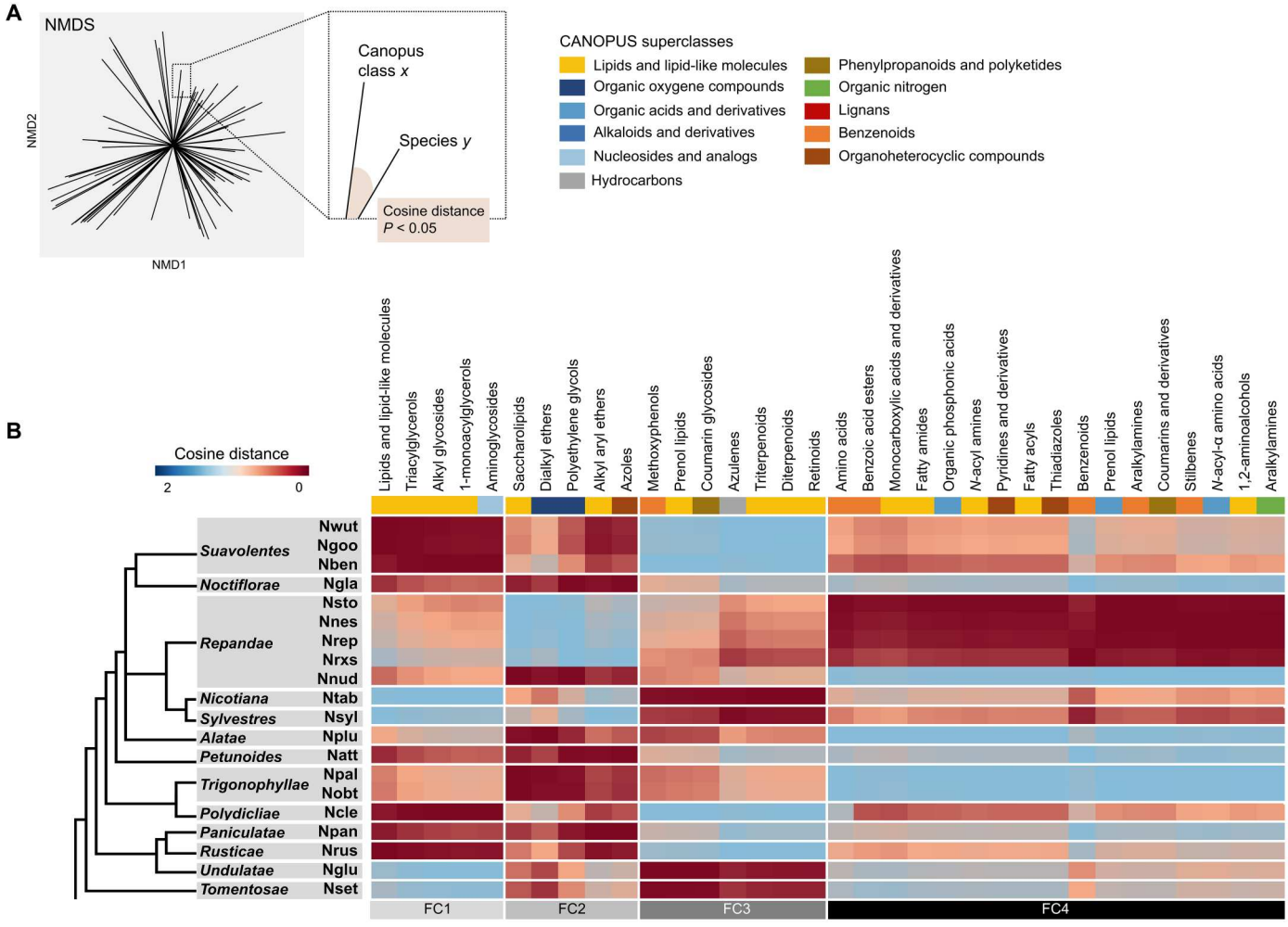

Fig. 4. NMDS reveals main statistical trends of *Nicotiana* section and species-level metabolic specialization. (**A**) NMDS was used to infer directionalities, followed by the calculation of intrinsic variables to test for statistical significance [*P* value (999 permutations) lower or equal to 0.05], in the association between species and CANOPUS superclass and most specific class predictions (CANOPUS; Fig. 3). All *P* values and cosine distances are summarized in data S2. (**B**) Heatmap representation (based on cosine distances) of statistically significant associations between species and NP-CANOPUS predictions for "most-specific classes" (colored according to top-level "superclasses"). A hierarchical clustering analysis was conducted to group similarly distributed CANOPUS predictions, thereby emphasizing on four highly distinctive clusters referred to as metabolic FCs.

(mono-/di-)acyl glucoses that dominate leaf exudates of *Suaveolentes* and *Rusticae* species. The combined examination of the multiple computational outputs demonstrated that these compounds co-occur at species level with above-mentioned acylglycerols, while acylsucroses are more broadly distributed within the *Nicotiana* genus (Fig. 6C).

NANNs as case study for structural diversity expansion in *Repandae* allopolyploids

In the following, we exemplify using the case study of NANNs on how the *Nicotiana* genus SM cartography and connected annotation resources can be exploited to gain (bio)chemical and evolutionary insights into specific SMs. NANNs have been described as leaf exudate allopolyploidy–mediated innovations specific to the *Repandae* section (*35*). In our data platform, NANNs' structural diversity was readily inferable from mass motif #433 (MC7) that included the two main nornicotine substructure molecular fragments at mass/charge ratio (*m/z*) of 132.0825 and at *m/z* 149.1075 (Fig. 7A). Inspection of this motif retrieved a far greater structural diversity than previously reported, with 102 of annotated NANNs, not counting noncanonical NANN structures with three N (NANNs integrating an aminated fatty acyl chain) or three O atoms (dihydroxylated NANNs) or those built on an anatabine scaffold instead of nornicotine (data S8). This NANN structural diversity directly translated from variations at the fatty acyl moiety level, with the presence of iso-/anteiso-branched or straight C_1 to C_{18} chains, with or without hydroxyl groups. As their structure had not been unambiguously identified in previous phytochemical reports (*35*), the most abundant hydroxy NANNs were purified and elucidated by nuclear magnetic resonance (NMR) to confirm the unusual position of the hydroxy group at position 3 (fig. S11 and Supplementary Text).

Total NANN pools were extremely high in leaf exudates and in trichome-rich calyces of the *Repandae* species but at barely

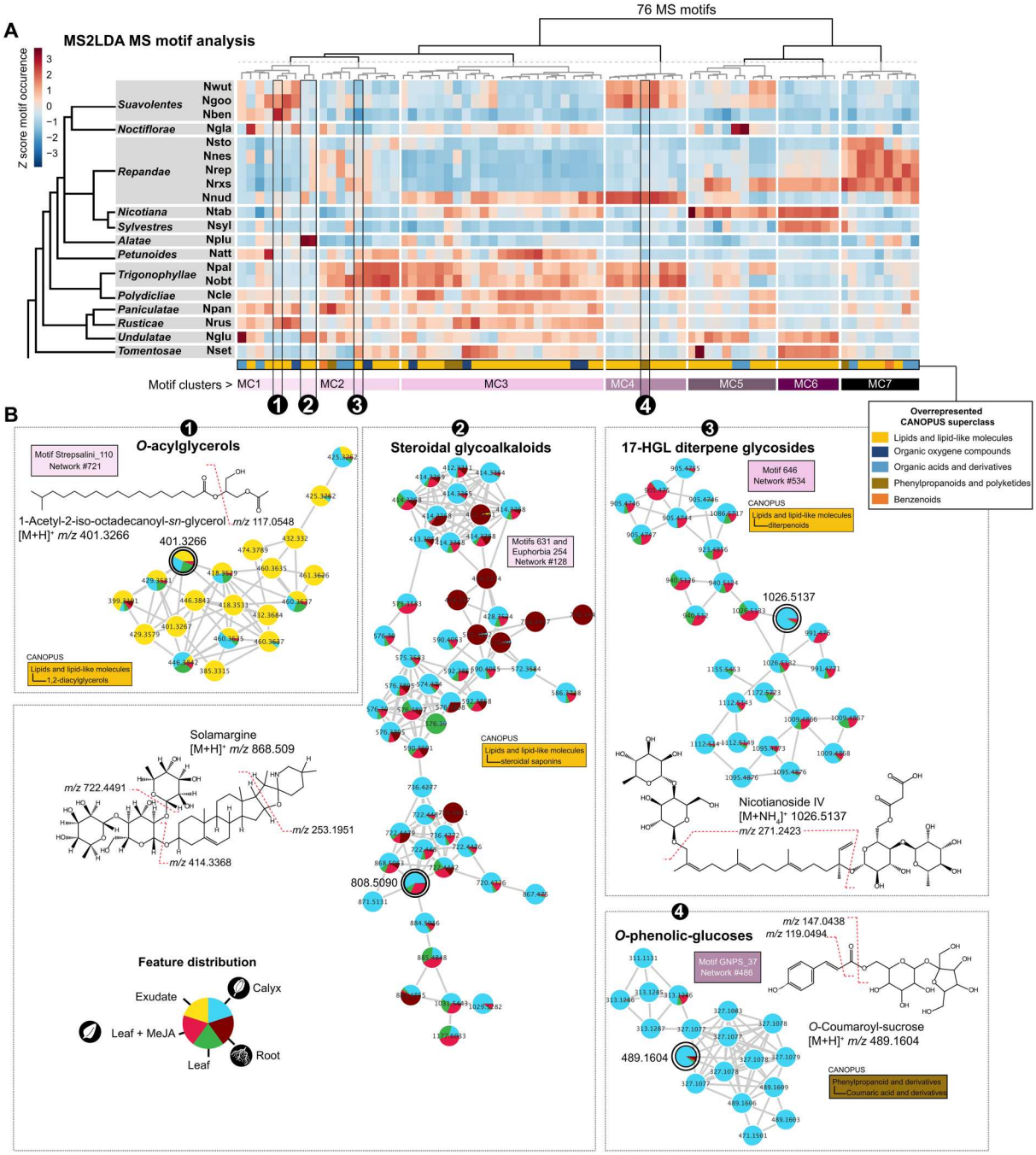

Fig. 5. A minimal set of MS motifs captures substructure diversity in *Nicotiana* chemotypes. (**A**) Hierarchical clustering analysis (HCA) based on the species-level motif count (*Z* score–normalized) of top 76 mass motifs inferred by unsupervised decomposition of overall MS spectra via the text-mining program MS2LDA. Species × tissue motif counts matrices can be explored within data S5. MCs extracted from the HCA approach refer to clusters of tightly covarying MS motifs. A principal component (PC) analysis (two first PCs) based on species-level MS motif relative intensity and loadings exerted on sample PC coordinates by each MS motifs, highlighted the strong resolving power for species grouping of these MCs (fig. S9). (**B**) Strategy for MS motif–guided exploration of substructure enrichment in particular molecular networks. MS motifs are selected on the basis of their peculiar species/section-level distribution, annotated using MS fragmentation curation and connected molecular network are lastly visualized. Node colors denote for the species-overall feature relative abundance in the analyzed tissues. Rectangles report network and MS motif IDs, and their colors refer to MC. A representative high-confidence predicted structure per network (connected to the double circled node) is presented with annotation of the MS motif main fragments. Additional examples are presented as part of fig. S10. Overall MS motif data are reported in data S6 and S7.

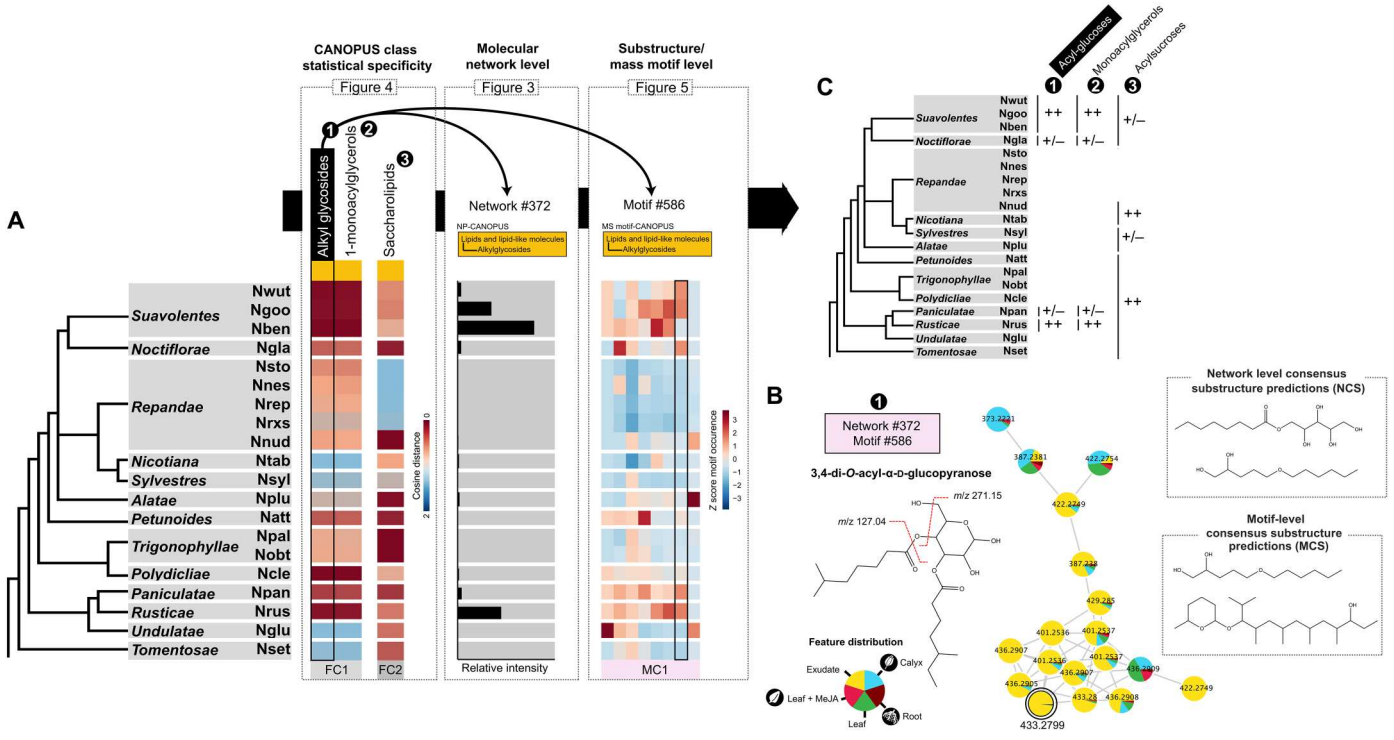

Fig. 6. An illustration of how to combine multilevel computational metabolomics outputs to assess leaf surface acylated sugars/glycerol diversification. (**A**) Workflow to interrogate species-level molecular network relative intensity (Fig. 3 and data S1), significant associations with NP-CANOPUS predictions for most-specific classes (Fig. 4 and data S2), and mass motif distributions (Fig. 5 and data S5) to unravel SM diversification patterns. Three NP-CANOPUS most-specific classes exhibiting significant species-level associations are initial selected for further examination: alkyl glycosides (*1*), 1-monoacylglycerols (*2*), and saccharolipids (*3*). A detailed examination of these, supported by the computational workflow, indicates that metabolites of the corresponding molecular networks relate to diacylglycerols, monoacylglycerols, and acylsucroses. As an example, NP-CANOPUS alkyl glycosides, which close association with the *Suaveolentes* and *Rusticae* sections, are overrepresented by network #372 [exemplified in (B)] and MS2LDA mass motif #372. The latter motif combines diagnostic fragments of a C_8 acyl group (fragment_127.1125) and glucose with a C_8-acyl group that lost two —OH groups (fragment_271.1525). (**B**) Molecular network #372 and predicted consensus substructures. The predicted consensus substructures for this network are alkyl chains with varying lengths. Consistently, associated consensus substructures (MCS) of mass motif #586 also display alkyl chains with varying lengths. Complete NCS and MCS data are accessible in data S3 and S6, respectively. Features of this network are specifically enriched within the leaf surface exudates (yellow). The proposed structure of the mass feature at *m/z* 433.2799 (bold circles) as a diacylated glucose derivative is highlighted with its explainable fragmentations above. (**C**) Distribution at the *Nicotiana* section level of main surface acylated sugars/glycerols as inferred from the computational workflow. ++, high abundance of the compound class; +/−, moderate abundance. Color keys for the different heatmaps in (A) are as implemented in the cited figures.

detectable levels in *N. nudicaulis* (Fig. 7B). Most unexpectedly, our data mining revealed that roots harbored a previously unexplored diversity of NANNs, albeit at almost two orders of magnitude lower than in leaves, and with very different chemotypes (Fig. 7B). In this respect, cross-tissue comparisons of fatty acyl moieties among NANN chemotypes indicated a general tendency toward shorter chain NANN (most notably C_8-nornicotine and formyl-[C_1]-nornicotine) accumulation in root tissues (fig. S12). A closer inspection of previously noted noncanonical NANNs captured by this exploratory approach led to the formulation of structural assignments for four structures harboring a second intrachain hydroxyl group and four additional ones bearing a third N atom as part of an intrachain amine group (Fig. 8A). These noncanonical NANNs were purified, but because of insufficient yields, their structure could not be further interpreted by NMR. In agreement with the presence of a third N prone to be positively charged, these noncanonical NANNs mainly appeared in the form of their $[M+2H]^{2+}$ and exhibited higher polarity than regular ones. Features corresponding to these noncanonical NANNs shared with canonical ones the mass motif #433 associated with the nornicotine backbone fragmentation but were located in different molecular networks (Fig. 8A) that were specific to the *Repandae* section (fig. S13). These *Repandae* noncanonical NANNs were further analyzed by ultrahigh-resolution matrix-assisted laser desorption/ionization (MALDI) MS imaging experiments conducted from leaf cross sections of *N. nesophila*. These analyses supported their uniform distribution within the leaf lamina, the corresponding MS imaging (MSI) images overlapping with those of well-known lamina-distributed SMs such as chlorogenic acid and not specifically on the leaf surfaces as for canonical NANNs (Fig. 8B and fig. S14).

Assessing NANNs evolutionary diversification

Our data strongly challenged the previous view that NANN biosynthetic capacity strictly arose as part of the allopolyploidy event at the base of the *Repandae* and that, hence, NANNs could be considered as a transgressive metabolic trait to this section. Figure 7 shows that the NANNs' diversity pervades the different *Nicotiana* sections, albeit at extremely low levels in all the species examined additionally to the *Repandae* section. Obviously, complete leaf extracts of *N. nesophila* (H = 3.25, 53 NANNs) and *N. repanda* (H = 3.17, 49

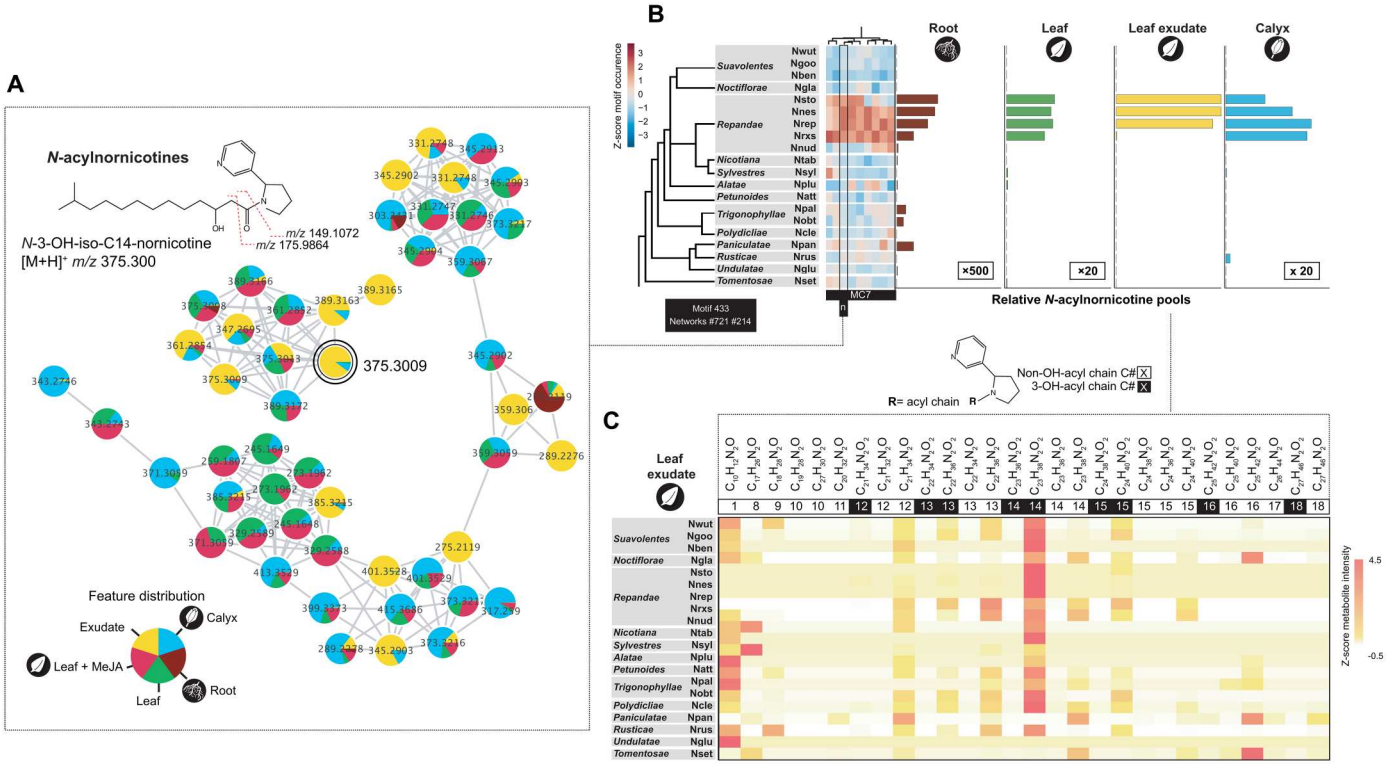

Fig. 7. Navigating MS motifs pinpoints on a diversity of NANNs that dominate leaf surfaces of *Nicotiana* section *Repandae* species. (**A**) Main molecular networks extracted connected to MS motif 433 (MC7; Fig. 5A) characterized by a strong relative abundance in *Repandae* species. NMR-elucidated NANN structure (see further NMR-elucidated NANNs in fig. S11), with fragment annotations captured by the NANN MS motif, for the MS/MS feature represented by the double circled node. Node colors denote for the species-overall feature relative abundance in the analyzed tissues. (**B**) Total NANN pools (relative to maximum in *N. nesophila* exudates) as inferred from MS/MS features of MS motif 433 (data S8). (**C**) Species-level NANN elemental formula distribution (*Z* score–normalized) and indication of the acyl chain length and of its 3-hydroxylation.

NANNs) exhibited the overall greatest NANN α-diversity values (fig. S15). Of all leaf exudate samples examined, the NANN α-diversity calculated for hybrid *N. repanda* × *sylvestris* (H = 3.03, 18 NANNs) was the highest, which reflected a balanced distribution among NANN relative intensities in this sample. By clear contrast, lowest NANN α-diversity values were detected for leaf exudates of *N. repanda* (H = 0.42, 24 NANNs), *N. stocktonii* (H = 0.39, 22 NANNs), and *N. nesophila* (H = 0.54, 24 NANNs), which further indicated, besides the high NANN biosynthetic capacity in these species, their exacerbated specialization toward C_{14}-OH-nornicotine exudation. In this respect, while the NANN chemotypes of the leaf exudates of almost all of the focal species were characterized by the dominance of this particular NANN, *N. rustica* and *N. setchellii* were noticeable exceptions, being dominated by C_{16}-nornicotine (Fig. 7C) and *N. glutinosa* for its exclusive accumulation of formyl-nornicotine. As previously noted (Fig. 7B), roots of almost all species harbored a rich diversity of NANN, particularly exacerbated in *N obtusifolia* (H = 2.26, 8 NANNs), predicted as one of the closest diploid progenitors to the *Repandae* section.

Together, a most parsimonious explanation to the evolution of the NANN pathway was that it predates *Repandae* formation (Fig. 9). Such an evolutionary scenario appeared to be supported in all tissue-level ancestral state reconstruction (ASR) analyses carried out based on a *matK*-based species tree and with total NANN levels expressed as discrete states (Fig. 9A). The ASR analysis computed from total root NANNs in combination with tissue-level NANN chemotypes further suggested that the last common ancestor to the examined species had a consequent root-based NANN accumulation capacity. In this respect, in all *Nicotiana* species, root-level NANN chemotypes consistently contrasted from shoot-level ones by their important proportion of C_8-acylated and minor levels of shorter fatty acyl chain NANNs (Fig. 9B). While other species such as the allotetraploid *N. rustica* exude moderate amounts of NANNs on their calyx surfaces (Fig. 7B), suggesting independent evolutionary events in the amplification of NANN production, the extremely high amounts of NANN exudation on both leaf and calyx surfaces constitute a character specific to the *Repandae* section (with the exception of *N. nudicaulis*).

DISCUSSION

Lineage-specific reconfigurations in rapidly evolving sectors of a plant specialized metabolism can be difficult to assess solely from genomics/transcriptomics data. This stresses the obvious fact that the power of genomics-driven evolutionary inferences on plant SM pathways critically relies on the chemical classification of metabolites part of these metabolic sectors and on the phylogenetics contextualization of this information. To tackle this issue, the open-source computational metabolomics approaches presented here are propelled by a broadly transposable multi-inference

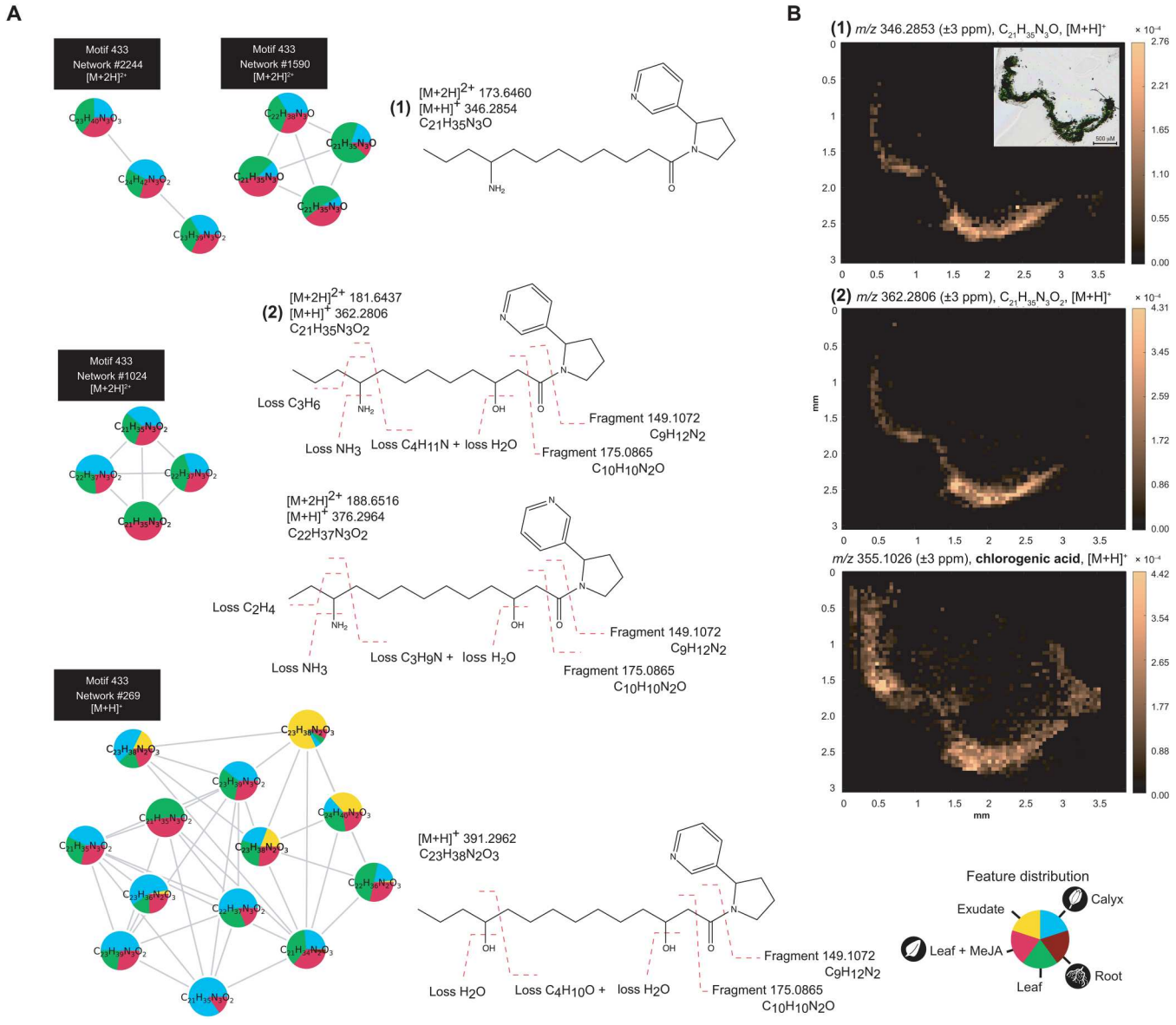

Fig. 8. Characterization of noncanonical leaf lamina NANNs specific to the *Repandae*. (**A**) Molecular networks and fragmentation characterization of 3N-containing and dihydroxylated NANN specific to the *Repandae* (fig. S13). Node colors denote for the species-overall feature relative abundance in the analyzed tissues. (**B**) MALDI MS images depicting spatially resolved relative abundance of selected metabolites in a leaf cross section of *N. nesophila*. Insert in the first image corresponds to the optical image of the matrix-embedded leaf cut used for MALDI MSI. The two first images correspond to the MSI data for two 3N-containing NANNs: *m/z* 346.2853 (±3 ppm, $C_{21}H_{35}N_3O$, $[M+H]^+$) and *m/z* 362.2802 (±3 ppm, $C_{21}H_{35}N_3O_2$, $[M+H]^+$) exhibiting a quasi-uniform distribution within the complete leaf section and comparable to that of chlorogenic acid (third image, *m/z* 355.1026 ± 3 ppm). Selected MSI data are presented for additional *N. nesophila* metabolites in fig. S14.

annotation approach that maximizes the coverage of substructure predictions, thereby resulting into an unprecedented cartography of SM diversity in the *Nicotiana* genus linking species-level SM prevalence to particular substructures. With this workflow, we notably shed light on the structural diversity and phylogenetics distribution of NANNs, a gain-of-function defensive innovation previously thought to have evolved with *Repandae* allopolyploids speciation (*38*).

A major challenge in MS metabolomics remains to reach broad structural annotation ("deep metabolome annotation") and substructure discovery beyond chemical class predictions and the dereplication of previously identified SMs, which is the most frequent outcome of molecular networking–based data exploration. In particular, with the use of heterogeneous computational annotation tools and that of querying highly diverse experimental and in silico MS/MS database comes the inherent difficulty of systemically prioritizing and/or merging the minimal set of most reliable annotations collected from these inferences. MolNetEnhancer has been developed to more efficiently combine outputs from molecular networking, MS2LDA as well as in silico and chemical classification tools (*45*). However, substructure discovery from MolNetEnhancer outputs is strongly hampered by the scarcity of annotated motifs in

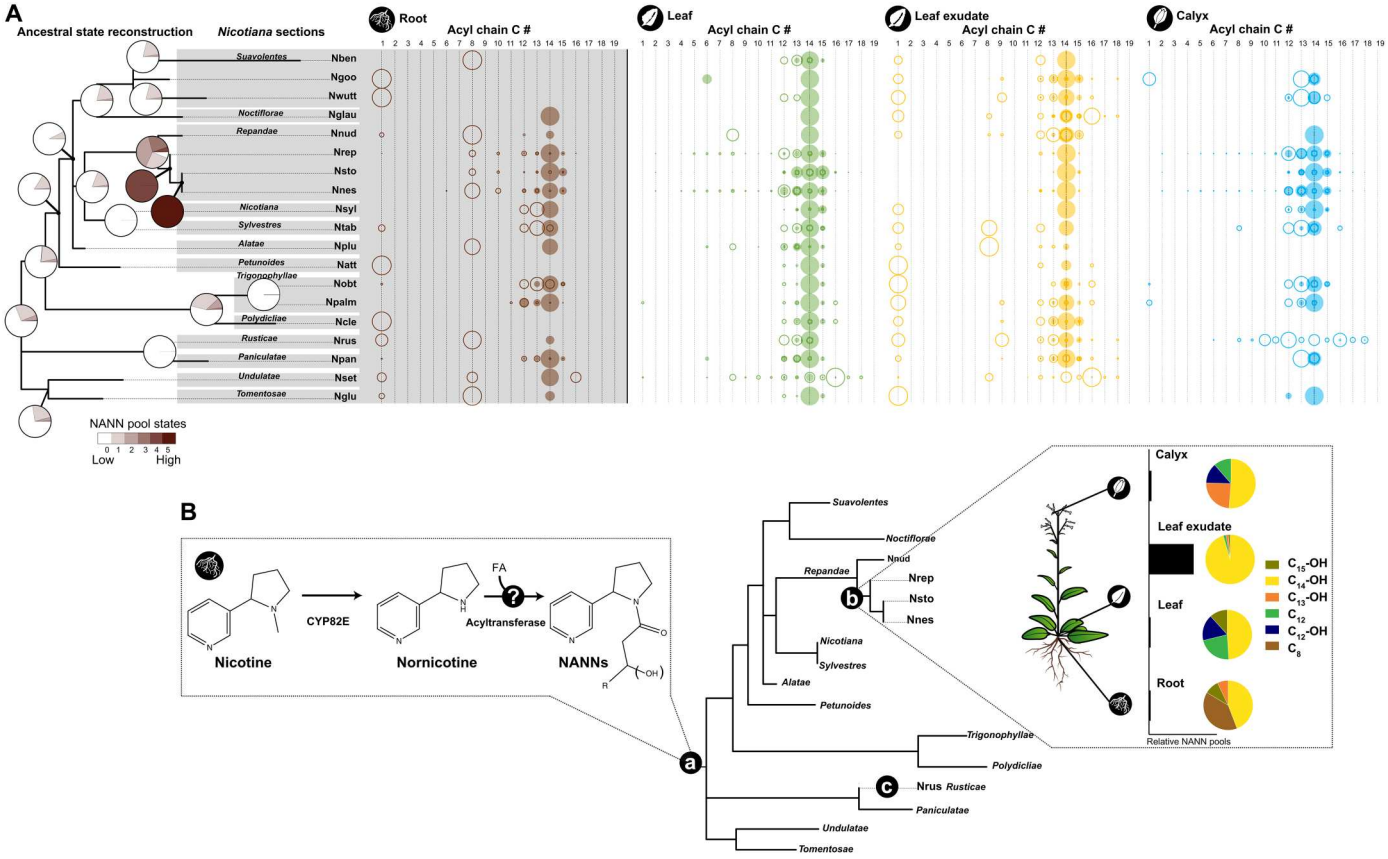

Fig. 9. ASR and structural diversity analysis indicate that NANNs predate *Repandae* speciation and a major root-to-shoot compositional shift. (**A**) Total root NANN pools of the focal species were transposed as relative scaling into an ordered trait (total states colored from white to dark brown) and used as input for ASR using the MBASR software with default settings. The species tree was constructed from *matK* as described in (*73*). Bubble plots on the right part of the figure depict relative NANN fatty acyl chain distribution with indication of fatty acyl chain carbon number (fig. S12); for total NANN pools, see Fig. 7B. Bubble size denotes for relative acyl chain level within the NANN pool of a species and per tissue. Color-filled bubbles refer to hydroxylated NANNs. (**B**) Main biological insights gained from the present computational metabolomics workflow on the NANN evolutionary diversification. Acquisition of the NANN biosynthetic capacity predates *Repandae* allopolyploid formation, but nornicotine *N*-acyltransferases responsible for the NANN structural diversity remain to be identified (a). While other species such as the allotetraploid *N. rustica* exude moderate amounts of NANNs on their calyx surfaces (c), suggesting independent evolutionary events in the amplification of NANN production, markedly high amounts of NANN production constitute a character specific to the *Repandae* section (with the exception of *N. nudicaulis*) (b). In all *Nicotiana* species, root-level NANN chemotype consistently contrasts from shoot-level ones by their important proportion of C_8-acylated and minor levels of shorter fatty acyl chain NANNs. Relative NANN pools and distribution presented in the bar chart and circular diagrams are from *N. repanda*. FA, fatty acid chain.

the Mass2Motifs database embedded into MS2LDA and by the fact that many of these correspond to relatively unspecific fragmentations (e.g., water, methyl, and hexose losses). Only 24 of the 76 mass motifs retained for further analysis had partial annotation hints in the MS2LDA Mass2Motifs database (data S5). To improve substructure discovery and annotation, we implemented two complementary approaches. On the one hand, we propagated CANOPUS predictions at mass motif level (MP-CANOPUS) by computing frequencies in "superclass/subclass/most specific class," and combined this information with mass motif coregulation analysis (Fig. 5). The second approach implemented for substructure analysis involved advanced maximum common substructure calculations to integrate annotations from multiple tools on a network (NCS) or motif level (MCS). Overall, we obtained 349 NCS or 303 MCS predictions for the whole dataset (data S3 and S6). Maximum common substructure computation for substructure prediction had been used in one of our previous studies to cluster candidate structures obtained by the MetFrag searches among coregulated herbivory-induced metabolites (*46*) and is also one of the processing steps within the Network Annotation Propagation tool of the GNPS web platform (*47*). Together, we advocate that the NCS/MCS approach implemented here has three main advantages: (i) It is an efficient mean of summarizing common substructure within the diversity of outputs from database queries as SMILES strings, (ii) it can used as input to reveal substructures statistically associated with intense chemodiversification in a given species, and (iii) it provides structural guidance during the manual interpretation of mass motifs or molecular network. In this respect, our study led to the curation of 76 mass motifs (data S5). Such an effort is important to empower supervised search of mass motifs, which is already possible in MS2LDA and which will be greatly facilitated with the recent release of the MS2QUERY tool (*48*).

A very important delivery of our work is the development and public sharing of the 1M-DB which is, to the best of our knowledge,

the largest in silico spectral database. This approach resulted into fivefold more hits (annotation of 57% of the total features) than experimental spectral database interrogation alone. Data of the 1M-DB can currently be accessed and interrogated from the GNPS platform. The size of this dataset can represent a challenge for MatchMS-based queries, which can nonetheless be locally implemented with reasonable computing capacity with the parallelized script (see the "Code availability" section) provided with our study. It is therefore foreseeable that the efficiency of the interrogation of the 1M-DB will strongly benefit from up-to-date optimization of MatchMS parallelization as part of future version releases. Multiple tools have been developed in recent years to produce hypothetical MS/MS spectra (*23*–*26*, *49*). A more recent development in this area is that of QCxMS, a computational tool that generate high-quality fragmentation spectra from molecules based on molecular dynamics calculations (*26*). This program is currently too much computationally demanding and could not be transposed to the scale of this study, besides the computation of MS/MS predictions for the 429 structures of the Jassbi database and using a limited number of fragmentation trajectories (Zenodo link: https://doi.org/10.5281/zenodo.8123590). One promising direction for improving the confidence of such in silico fragmentation–based annotation is exemplified by the recently developed COSMIC workflow that incorporates a confidence score consisting of kernel density *P* value estimation from a decoy library and a support vector machine algorithm (*50*). With the increasing quality of MS/MS predictions, one interesting perspective could be to extract mass motifs from them and thus directly infer fragment substructures produced from known structure in silico decomposition.

In terms of structural information, the SM metabolic cartography generated in this study goes far beyond to a recently published chemotypic classification of the *Nicotiana* genus that mostly consisted in the dereplication of primary metabolites such as steroids and only a few SMs (*51*). In our opinion, this data platform and our SM cartography provide complementary views on the metabolic diversity of this genus. Noteworthy, the aforementioned study did solely focus on leaf metabolomes, while ours and previous studies (*8*) unambiguously indicated the importance of "screening" multiple tissues to capture a broader SM diversity picture. In this respect, we demonstrated that expanding the analysis at the multitissue level (by combing tissue-level molecular network information) resulted into a phylometabolomics tree that captured shared SM biosynthetic potential among closely related species with more resolution (Fig. 2). Beyond simple presence/absence of SM classes, which has been a traditional focus of chemotaxonomic studies, the fact that structural diversity can nowadays be more efficiently accessed with computational MS metabolomics opens research avenues for understanding the evolution of SM, as implemented in a recent survey of the SM synapomorphies and homoplasies in the Malpighiaceae family (*52*). Information theory Shannon statistics transposed to MS feature analysis or individual metabolites can also provide an efficient means of contrasting metabolic diversity among the metabolic profiles to examine evolutionary ecology theories and contextualize those at relevant taxonomic scales (*53*). By using α-diversity analysis, we confirmed that roots exhibit, under our analytical conditions, the most specific metabolomes, a pattern that had been previously detected in a study focusing on *N. attenuata* as the sole model species (*8*). α-Diversity scores further varied in-between species, thereby indicating variations in constitutive SM biosynthetic capacities and/or constitutive versus stress-induced investments into SM production. In this respect, we further observed that these interspecies variations in MeJA inducibility were negatively correlated with α-diversity scores constitutive leaf metabolome (Fig. 2B). This trend is reminiscent of the interspecies patterns detected from the comparative analysis of early herbivory-induced transcriptomes for six *Nicotiana* species (*54*) and may reflect physiological trade-offs between constitutive versus inducible metabolic diversity maintenance.

Many interesting biochemical insights worth to be pursuing by gene function studies were extracted from the SM cartography produced from this study. Our analysis notably detected the presence of mono-*O*-acylglycerols (classified under the CANOPUS most specific class 1-monoacylglycerols) specifically on the leaf surfaces of the section *Suaveolentes* and at lower abundances in the *Rusticae*. Besides its well-known housekeeping function in the synthesis of di- and tri-*O*-acylglycerols via the action of glycerol 3-phosphate acyltransferase enzymes (*55*), the latter compound class has been poorly investigated regarding its presence on plant aerial surfaces. Main reports on the possible defense-related functions of this compound class derive from studies on their presence as abundant surface metabolites on the calyx of several Scrophulariaceae species (*56*) and from a unique report for the *Nicotiana* genus describing these compounds as efficient chemical glues against small insects on the leaf surfaces of *N. benthamiana* (*57*). The prevalence of this compound class in the *Suaveolentes* section, particularly in *N. benthamiana*, could point to an interesting case study to functionally examine the biochemistry and evolution of this pathway and compare it with that of the thoroughly investigated and structurally reminiscent acylsugars (*11*). Our analysis also revealed subtle tissue-level chemotypic variations within *O*-acylsugar networks. Apart from confirming previously detected strong cross-species variations in structural diversity, inspections of these networks also indicated that some of these acylsugars are present at low levels in roots (fig. S10). This could further illuminate recent work on the predicted role of these SMs in plant-soil microbiome interactions (*15*). We further exemplify how multilevel computational inferences retrieved from our approach can be combined to provide additional insights on the evolutionary diversification of acylsugars/glycerols within the *Nicotiana* genus (Fig. 6). In this case study, (mono-/di-)acyl glucoses inferred from our approach appeared present at high levels in the *Suaveolentes* and *Rusticae* sections, a distribution contrasting with that of well-characterized acylsucroses. Acyl glucoses have been previously reported from *N. benthamiana* and *Nicotiana miersii* (*57*, *58*) but are most well characterized from wild tomato *Solanum pennellii*, in which their biosynthesis has been linked to the activity of a specific invertase enzyme (*59*). These compounds have also been described in *Datura* species, and functional genomics work further indicated signatures of convergent evolution of the underlying biosynthetic pathway in the *Solanum* and *Datura* genera (*60*). It would be of great interest to study which regulatory mechanisms contribute to the species-level co-occurrence of this compound class with monoacylglycerols, as well as the biosynthetic underpinnings to this compound class in *Nicotiana*, since its distinctive distribution could be shaped by reconfigurations of invertase activity in trichomes (*59*).

Our SM cartography also provided species × tissue resolution on terpene-related classes' distribution previously examined in *Nicotiana* studies that targeted trichome-based cembrene diterpene (*61*)

and 17-HGL-DTG (*6*). Our study revealed for these two classes of diterpenes, pronounced expansions of structural diversity and significant associations with the *Nicotiana*, *Sylvestres*, *Undulatae*, *Tomentosae*, and *Trigonophyllae* (17-HGL-DTG) sections that include species in which emblematic structures of these compound classes had been originally detected (*6*). An unexpected result was the detection, at large levels in *N. plumbaginifolia* and to a minor extent in *N. glutinosa*, of steroidal glycoalkaloids, emblematic of the *Solanum* genus, and whose presence is considered as erratic in other Solanaceae genera. Within the structurally rich network of steroidal glycoalkaloids identified in our study, the dereplication of solaplumbin *m/z* 722.4479, ($[M+H]^+$, $C_{39}H_{64}NO_{11}$) is supported by old phytochemistry reports (*62*). This unexplored patchy distribution of steroidal glycoalkaloids within the Solanaceae provides exciting foundations for future evolutionary biochemistry studies. Consistent with the exploratory power of the presented approach, we further detected a largely uninvestigated network of root-enriched glucoside derivatives of nicotine and possible nicotine biosynthetic intermediates (fig. S16).

An interesting perspective is to decipher metabolic reconfigurations that are associated with allopolyploidy events within the *Nicotiana* genus. The present study design does not allow, because of the absence of certain diploid progenitor species (*Nicotiana tomentosiformis* in the case of *N. tabacum* and *Nicotiana undulata* in the case of *N. rustica*), to systematically compare metabolic distances between allotetraploid metabolomes and those of closest diploid progenitors (table S2). Taking into account this limitation, However, note that we did not observe a tendency for greater α-diversity scores, calculated from whole metabolome data, in allotetraploid species as compared to diploid species. This further indicates the importance of analyzing allopolyploidy-mediated metabolic modulations at the compound class level. Results of these analyses could be reminiscent of the complex reconfigurations detected in a previous study assessing floral morphological and associated metabolic trait variations in *Nicotiana* allotetraploids (*34*). Because of their previously reported absence in *Repandae* closest diploid progenitors (*N. sylvestris* and *N. obtusifolia*), NANNs have often been considered as "transgressive" metabolic traits derived from the *Repandae* allopolyploidization. In our study, we annotated 102 NANNs, including six first elucidations by NMR and found NANN-related structures built from anatabine as a backbone, as well as the presence of leaf lamina–based NANNs restricted to *Repandae* that contain uncommon aminated fatty acyl moieties. Above all, our study indicates that the NANN biosynthetic capacity predates the *Repandae* section formation. However, a main innovation of *Repandae* species is their capacity to accumulate very high level of canonical NANNs on their surfaces and N_3-containing NANNs in their leaf laminas (Fig. 8). These data provide rigorous support to old literature that reports anecdotal evidence (*63*, *64*) for low amounts of short (−formyl, −acetyl) and middle (C_4 to C_8) chain length NANNs present in other *Nicotiana* species (*65*). *N. obtusifolia*, considered as a closest extant female progenitor to *Repandae*, is one of the *Nicotiana* species that accumulates the largest nornicotine-to-nicotine ratio in its leaves (*66*). Another interesting observation to pursue is that *N. sylvestris*, the closest extant male progenitor to *Repandae*, is thought to have contributed to several allopolyploidization events in the genus *Nicotiana*, many of which being able to accumulate greater NANN amounts than the other species tested in this study. Hence, our data, as presented in the summary model of Fig. 9B, suggest a more complex than previously thought evolution of the NANN pathway.

In particular, a cornerstone biochemical perspective to this work will be the identification of the NANN biosynthetic *N*-acyltransferase(s), which is predicted to be abundant in *Repandae* trichomes from our data and from previous phytochemical analyses on crude trichome fractions (*35*–*37*, *67*). Building on the strategy successfully used for the characterization of BAHD (named after the first four biochemically characterized acyltransferases BEAT, AHCT, HCBT, DAT) enzymes responsible for the diversity of trichomes acylsugars in Solanaceae species (*11*), comparative transcriptomics analyses are currently ongoing to pinpoint on candidate nornicotine *N*-acyltransferases. Previous studies on acylsugar biosynthesis further indicated that intra- and interspecific variations in acylsugar chemotypes are controlled by subtle modulations of BAHD gene expression and enzyme acyl acceptor affinity (*11*). The identification of nornicotine *N*-acyltransferase(s) will pave the way for mechanistic investigations on the evolutionary diversification of NANNs in the *Nicotiana* genus and on specificities underpinning trichome-level flux capacity amplification in the *Repandae* and to a much more moderate extent in *N. rustica*.

Last, our tissue cartography revealed a largely unexplored repertoire of NANNs in the roots of all examined species with an important proportion of C_8-acylated and minor levels of shorter fatty acyl chain compounds (Fig. 9B). These data and ASR analyses are in favor of shorter chain NANN production in roots being a most ancestral trait in this metabolic class. In the context of the above-mentioned future biochemical investigations, the latter interpretation would be consistent with the fact that the accumulation of canonical NANNs onto aerial surfaces involves trichome-based *N*-acyltransferase enzymes with greater affinity for long-chain fatty acyl–coenzyme A as compared to those present in roots.

In conclusion, the fully open data and broad range of data integration approaches and provided here present an unprecedented resource to revive SM analysis in the *Nicotiana* genus and contribute to the establishment of phylometabolomics as an instrumental bottom-up approach to guiding future evolutionary biochemistry studies.

MATERIALS AND METHODS

Plant material, growth conditions, and treatment

Nicotiana species with their origin and associated accession numbers are summarized in table S1. Seeds of all *Nicotiana* species were directly germinated on soil, with the exception of *N. attenuata*, for which smoke-induced seed germination was established as described previously (*8*). For all species, glasshouse growth conditions were as described previously (*8*). Six- to eight-week-old elongated plants were used for all metabolomics analyses. To analyze the regulatory function of jasmonate signaling on metabolomics-inferred specialized metabolism classes, petioles of two elongated plants were treated with either 20 μl of lanolin paste containing 150 μg of MeJA (Lan + MeJA) or with 20 μl of pure lanolin (Lan) according to Heiling *et al.* (*6*). Leaf samples were harvested 72 hours after treatment, flash-frozen in liquid nitrogen, and stored at −80 °C until use.

Metabolite extraction procedures for UPLC-QTOF MS

Leaf, root, and calyx metabolites were extracted for UPLC-QTOF MS analysis as previously described (*6*). Briefly, for leaf samples, 12 discs per plant (~100 mg of fresh-weight tissue) were flash-frozen in liquid nitrogen immediately after harvest and stored at −80 °C until use. The latter frozen leaf samples were ground in a Tissue Lyzer II for 3 min at 30 Hz, and metabolites were extracted by addition of 1 ml of 80% methanol and 1 hour of shaking at 1000 rpm at 4 °C and further kept with a gentle agitation overnight at 4°C. Samples were lastly centrifuged for 10 min at 14,000*g*, and the resulting supernatants were transferred into glass vials. Root samples referred to the complete root system of about 8-week-old plants. After soil removal, roots were rinsed in water, gently dried with paper towels, and flash-frozen in liquid nitrogen. Root samples were homogenized in a Tissue Lyzer II for 4 min at 30 Hz. Metabolite extraction was conducted as above described from 200 to 400 mg of root material (primary, secondary, and tertiary roots). Flower calyces were collected from about 8-week-old plants and processed for metabolite extraction using above leaf metabolite extraction conditions. To obtain leaf exudates enriched into semipolar to apolar surface metabolites, fully elongated leaves were briefly rinsed with acetonitrile. These exudates were filtered on filter paper and completely dried under reduced pressure. Dried residues were then redissolved in methanol, and total metabolite concentration was adjusted to 1 mg/ml, except for *N. repanda*, *N. stocktonii*, and *N. nesophila* exudates that were diluted to 0.001 and 0.1 mg/ml (see table S1) to avoid detector saturation, due to the high levels of NANNs in these samples. Peaks areas were corrected by corresponding dilution factors.

UPLC-QTOF MS chromatographic conditions

Methanolic extracts were analyzed using ultrahigh-pressure liquid chromatography coupled to high-resolution MS on an UltiMate 3000 system (Thermo Fisher Scientific) coupled to an Impact II (Bruker) QTOF spectrometer. Chromatographic separation was performed on an Acquity UPLC BEH C18 column (2.1 × 100 mm, 1.7 μm; Waters) equipped with an Acquity UPLC BEH C18 precolumn (2.1 × 5 mm, 1.7 μm; Waters) and using a gradient of solvents A (water, 0.1% acetonitrile, and 0.05% formic acid) and B (acetonitrile and 0.05% formic acid). Chromatography was carried out at 35°C with a flux of 0.4 ml/min, starting with 10% B for 3 min and reaching successively 20% B at 12 min, 35% B at 17 min, 40% B at 23 min, 45% B at 25 min, 50% B at 30 min, and 95% B at 40 min, holding 95% for 5 min and coming back to the initial condition of 10% B in 3 min. These chromatographic conditions (total running time of 48 min) were previously optimized for the comparative metabolomics of methanolic extracts of Solanaceae species in one of our previous studies (*6*). Samples were kept at 4°C during the sequence of injections, and 5 μl per sample was injected in full-loop mode with a washing step after sample injection involving 150 μl of the wash solution (water:methanol, 80:20, v/v).

Conditions for data-dependent acquisition MS/MS data collection during UPLC-QTOF MS analysis

The Impact II QTOF instrument was equipped with an ESI source and operated in positive ionization mode on a 50- to 1500-Da mass range with a spectrum rate of 5 Hz and by further using the AutoMS/MS fragmentation mode. The end plate offset was set at 500 V, capillary voltage at 4500 V, nebulizer at 2 bar, dry gas at 10 liters/min, and dry temperature at 200°C. The transfer time was set at 60 to 70 μs and MS/MS collision energy at 80 to 120% with a timing of 50 to 50% for both parameters. The MS/MS cycle time was set to 2 s; absolute threshold was set to 31 counts per second (cts); active exclusion was used with an exclusion threshold at three spectra, released after 1 min; and an ion was reconsidered as precursor for the fragmentation if the ratio current intensity/previous intensity was higher than 5. MS/MS collision energy was set according to the mass from 25 V for a mass of 100 Da to 50 V for a mass of 1500 Da. The MS/MS spectrum acquisition rate was further optimized, from 3 to 7 Hz, according to the intensity of the observed mass. A calibration segment was included at the beginning of the runs allowing the injection of a calibration solution from 0.05 to 0.25 min. The calibration solution used was a fresh mix of 50 ml isopropanol:water (50:50, v/v), 500 μl of 1 M NaOH, 75 μl of acetic acid, and 25 μl of formic acid. The spectrometer was calibrated on the $[M+H]^+$ form of reference ions (57 masses from *m/z* 22.9892 to *m/z* 990.9196) in high precision calibration mode with an SD below 1 part per million (ppm) before injections, and recalibration of each raw data was performed after injection using the calibration segment.

Ultrahigh-resolution MS imaging data acquisition and processing

Freshly collected rosette leaves of *N. nesophila* were embedded into M-1 embedding matrix (Thermo Fisher Scientific) and frozen before cutting. Cuts were done on a transverse plane at 25 μm in thickness and −15°C using a cryotome FSE. Sections were deposited on indium-tin-oxide–coated slides and sprayed with a-cyano-4-hydroxycinnamic acid (HCCA) matrix at 10 mg/ml in 70% acetonitrile (ACN) and 0.1% trifluoroacetic acid using the HTX M5 sprayer. Nozzle temperature was set at 75°C, flow rate at 0.120 ml/min, velocity at 1200 mm/min, pressure at 10 psi, gas flow rate at 3 liters/min, and nozzle height at 40 mm. Four passes were applied with a track spacing of 3 mm and a HH pattern.

Samples were analyzed with a Burker SolariX 7 T Fourier transform ion cyclotron mass spectrometer at resolving power R = 120,000 at m/z = 400. Acquisition was performed in positive ion mode on a 100 to 500 *m/z* mass range, with an accumulation of 0.020 s, the transfer optics time-of-flight set at 0.600 ms, frequency at 6 Hz, and radio frequency amplitude at 350 Vpp. The MALDI plate offset was set at 100 V, deflector plate at 200 V, laser power at 20%, laser shots at 100, and frequency at 1000 Hz with a small laser focus. The instrument was calibrated by multipoint correction using the peaks of the HCCA matrix (*m/z* = 379.0924, 399.0377, 401.0744, and 417.0483). The regions of interest were determined in FlexImaging with a raster width of 50 μm. Images of the ions of interest ± 3 ppm were displayed in MSiReader v1.03 (*68*). The data were submitted to METASPACE and are available at https://metaspace2020.eu/project/nicotiana_msi-2022.

Feature-based molecular networking of UPLC-QTOF MS data

Raw data were converted to the .mzML format using MSConvert (version 3.0.21112-b41ef0ad4) (*69*). The resulting data files were then processed with the Batch Mode (see "Code availability" section, script S10) of MZMine 2.53 (*70*) and exported for FBMN analysis in the GNPS environment (*18*, *19*) and for spectral analyses in Sirius. The resulting .mgf and .csv files were further filtered to

exclude redundant nonbiologically informative MS/MS features using developed Python scripts S11 and S12 (see "Code availability" section). The *m*/*z* signals that appear >5 times (±3 ppm) with a retention time coefficient of variation greater than 10% were discarded. This filtering step excluded 11,580 features (of a total of 29,481 retrieved from the MZMine-based processing), a vast majority of those corresponded to redundant features detected at high level in solvent blanks. Last, FBMN was performed using the modified cosine as spectral similarity metric and with standard settings (version release_28.2, except lower precursor and fragment tolerance of 0.005 Da). Output of the FBMN analysis is available on GNPS at the following link: https://gnps.ucsd.edu/ProteoSAFe/status.jsp?task=cf822b6c7c914206941bb0b6007e7eb0.

MS/MS elemental formula and compound class predictions with Sirius

Sirius (version 4.8.2) was used to predict elemental formulas for MS/MS precursors and for the deep neural network–based compound class prediction as part of the CANOPUS pipeline (*20*, *21*). Sirius commands are summarized as part of script S13 (see "Code availability" section). Elemental formulas by Sirius were further processed with scripts S14 and S15 (see "Code availability" section) to restore feature IDs and calculate the degree of unsaturation of these formulas. A main strength of CANOPUS-based class prediction is that it does not involve the interrogations of spectral libraries with fragmentation spectra, thereby allowing class prediction of MS/MS features for which no database hit is retrieved and circumventing the possible issue of error propagation when false class prediction is obtained by FBMN network-level propagation from feature-derived database hits. MS/MS feature-level ontologies were retrieved from CANOPUS predictions as well as FBMN network-propagated superclass, subclass, and most specific class ontologies. The latter ontology propagation was implemented using script S19.

Mass motif inference by MS2LDA

Mass motifs were inferred using standard settings of MS2LDA (version release_23.1) (*22*), submitted through the GNPS workflow (available at https://gnps.ucsd.edu/ProteoSAFe/status.jsp?task=6f325f462e1145bfb465c679c2ee17d6). A total of 609 motifs were assigned including already existing motifs from motifdb. To explore mass motifs assignments on a species level, a binary mass motif matrix for all tissues was created by setting features above peak area of 10,000 to the value of 1 and those below to 0 (script S17). The resulting matrix was combined, and presence was summed per tissue and then set again into a binary matrix. Following this binary transposition of motif distributions, feature presence per motif was determined per species, resulting in a motif count table (script S18). This set of mass motif counts (after filtering and manual curation 76 motifs) was then normalized by motif ID and clustered by hierarchical clustering using the Ward clustering method implemented in MetaboAnalyst (*71*).

MS/MS annotation based on spectral database interrogations

We implemented a three-pronged approach to annotating MS/MS from the interrogation of experimental and in silico fragmentation databases, similar as proposed in Sumner *et al.* (*41*). Level 1 in our priority assignment of annotations corresponded to hits retrieved from experimental spectral databases and/or NMR structural confirmation. Highest priority within level 1 of annotated spectra (level 1a) was given to hits confirmed by NMR in this work. Level 1b annotations correspond to hits from spectral alignments (and correspondence of precursor *m*/*z* values) using a local MatchMS (score above 0.65 and >6 matching peaks) implementation (script S8, see "Code availability" section) with the modified cosine score, from an in house high-resolution experimental MS/MS spectra database of *N. attenuata* SMs and/or manual inspection of spectra. Level 2 corresponded in our annotation approach to hits retrieved, with the cosine score from high-resolution MS/MS spectra of the GNPS database. Level 3 annotations were considered for hits from alignments with in silico MS/MS spectra or in the case of network propagation of hits from the experimental databases, both after manual inspection. Jobs for the recently developed molDiscovery approach (version 1.0.0) (*24*) were submitted through GNPS with both the molDiscovery built-in library and the Jassbi compound database created as part of this study. The Jassbi compound database (429 structures) was compiled from structures extracted from a recent *Nicotiana* phytochemistry review (*32*). In silico MS/MS spectra for the Jassbi compound database were also produced with the fragmentation tool CFM-predict 4.0 (*23*) (script S5, see "Code availability" section) database searching was performed with MatchMS (*72*) (script S9).

Consensus substructure and molecular network chemical classes

We implemented an algorithmic approach to deal with the high number of annotations retrieved from the various in silico MS/MS spectral databases. To this end, we used annotations retrieved form Sirius (confidence score above 0.65), 1M-DB searched with modified cosine (score above 0.5 and 5 matching peaks), 1M-DB searched with spec2vec (score above 0.5), Jassbi-CFM (score above 0.5 and 5 matching peaks), and Jassbi-molDiscovery. These annotations were retrieved at the molecular network or at the MS2LDA mass motif level to calculate consensus substructures for a given network (NCS) or mass motif (MCS). Main steps involved in consensus substructure calculations involved the following commands (scripts S16 and S19, see "Code availability" section): (i) fragment structures, (ii) get the most common fragments, (iii) select the top 50 and only keep the ones with >12 atoms, (iv) cluster by structural similarity, (v) sort by cluster size, (vi) calculate the maximum common substructure within the cluster, and (vii) retrieve the top 4 results.

To harness the vast amount of structural information classified by molecular networking, we selected the top 252 networks sorted by only picking networks containing >10 nodes. The peak areas within these networks were summed with script S24. Peak areas were normalized (Excel's STANDARDIZE function) by cluster ID, and the maximum on tissue level per species was kept. The propagated CANOPUS classes were grouped their peak areas summed (script S28), and the resulting data were used to create per species treemaps in Excel. A summary of the top 252 molecular networks, their calculated consensus substructures, and their propagated CANOPUS classes can be found in data S3. In addition, data S4 and S7 allow the navigation of this multilevel information at mass motif and network levels.

Computing MS/MS-informed phylometabolomics species trees

To create MS/MS similarity-based species, referred to in Results as phylometabolomic trees, we used the data compiled as mentioned above (script S24) (Fig. 2A) or the data from the motif count (script S18) (fig. S9) to calculate the Euclidean pairwise distances between species' metabolomes (script S20). The resulting matrix was then used to plot trees in R with the APE package using the neighbor-joining algorithm and bootstrapping 999 with iterations (script S21).

ASR for the relative occurrence of NANNs

We adapted the concept of ASR classically used for the evolutionary analysis of quantitative phenotypic traits for the exploration of NANNs' relative occurrence. To this end, we first constructed a phylogenetic tree of the focal *Nicotiana* species–based sequences of the *matK* gene obtained from a previous study (*73*), the sequence of *Nicotiana maritma* was used to account for *Nicotiana wuttkei* position within the species tree due to unavailable genome data for the latter species. Laskowska and Berbec (*74*) previously suggested the very close relationship between the latter two species and reported their successful hybridization in the wild. *Nicotiana setchelli matK* gene sequence was obtained from the assembly of transcriptomics data publicly available for National Center for Biotechnology Information Sequence Read Archive accession SRR2106530. The species tree was constructed using NGPhylogeny.fr (*75*) with default one click options and the PhyML maximum likelihood method. For ASR, feature intensities accounting for the species and tissue-wide NANN diversity were retrieved using the above-described mass motif characterization approach. ASR was performed with the MBASR package (*76*) (script S25) on peak areas of the root that have been transformed into an ordered trait of five categories (Fig. 9 and fig. S1).

α-Diversity analysis and CANOPUS class distance computation

The α-diversity was calculated for each species based on Shannon entropy (script S29) using the scikit-bio package and sample features as operational taxonomical units. The top 252 networks as mentioned previously were selected their raw peak areas summed on the basis of propagated CANOPUS classes (script S28) and then converted to integers; networks without class annotations were discarded. The vegan package was used to perform NMDS, followed by the calculation of intrinsic variables (CANOPUS classes) with 999 permutations (script S30). The resulting vectors were used to calculate the per species cosine distances (script S31).

Code availability

All scripts used in this study are available on Zenodo, https://doi.org/10.5281/zenodo.8123590, and at the following GitHub repository: https://github.com/volvox292/Nicotiana_metabolomics.

Supplementary Materials

This PDF file includes:
Supplementary Text
Figs. S1 to S16
Tables S1 to S3
Legends for data S1 to S8
References

Other Supplementary Material for this manuscript includes the following:
Data S1 to S8

REFERENCES AND NOTES

1. H. A. Maeda, A. R. Fernie, Evolutionary history of plant metabolism. *Annu. Rev. Plant Biol.* **72**, 185–216 (2021).
2. M. Pigliucci, Phenotypic integration: Studying the ecology and evolution of complex phenotypes. *Ecol. Lett.* **6**, 265–272 (2003).
3. S. R. Whitehead, E. Bass, A. Corrigan, A. Kessler, K. Poveda, Interaction diversity explains the maintenance of phytochemical diversity. *Ecol. Lett.* **24**, 1205–1214 (2021).
4. D. Li, E. Gaquerel, Next-generation mass spectrometry metabolomics revives the functional analysis of plant metabolic diversity. *Annu. Rev. Plant Biol.* **72**, 867–891 (2021).
5. K. B. Kang, M. Ernst, J. J. J. van der Hooft, R. R. da Silva, J. Park, M. H. Medema, S. H. Sung, P. C. Dorrestein, Comprehensive mass spectrometry-guided phenotyping of plant specialized metabolites reveals metabolic diversity in the cosmopolitan plant family Rhamnaceae. *Plant J.* **98**, 1134–1144 (2019).
6. S. Heiling, S. Khanal, A. Barsch, G. Zurek, I. T. Baldwin, E. Gaquerel, Using the knowns to discover the unknowns: MS-based dereplication uncovers structural diversity in 17-hydroxygeranyllinalool diterpene glycoside production in the Solanaceae. *Plant J.* **85**, 561–577 (2016).
7. M. Itkin, U. Heinig, O. Tzfadia, A. J. Bhide, B. Shinde, P. D. Cardenas, S. E. Bocobza, T. Unger, S. Malitsky, R. Finkers, Y. Tikunov, A. Bovy, Y. Chikate, P. Singh, I. Rogachev, J. Beekwilder, A. P. Giri, A. Aharoni, Biosynthesis of antinutritional alkaloids in solanaceous crops is mediated by clustered genes. *Science* **341**, 175–179 (2013).
8. D. Li, S. Heiling, I. T. Baldwin, E. Gaquerel, Illuminating a plant's tissue-specific metabolic diversity using computational metabolomics and information theory. *Proc. Natl. Acad. Sci. U.S.A.* **113**, 7610–7618 (2016).
9. S. Meldau, M. Erb, I. T. Baldwin, Defence on demand: Mechanisms behind optimal defence patterns. *Ann. Bot.* **110**, 1503–1514 (2012).
10. R. Schuurink, A. Tissier, Glandular trichomes: Micro-organs with model status? *New Phytol.* **225**, 2251–2266 (2020).
11. G. D. Moghe, B. J. Leong, S. M. Hurney, A. Daniel Jones, R. L. Last, Evolutionary routes to biochemical innovation revealed by integrative analysis of a plant-defense related specialized metabolic pathway. *eLife* **6**, e28468 (2017).
12. O. Servettaz, A. Pinetti, F. Bellesia, L. B. Maleci, Micromorphological and phytochemical research on *Teucrium scorodonia* and *Teucrium* siculum from the Italian Flora. *Bot. Acta* **107**, 416–421 (1994).
13. Y. Sun, T. Guo, F. Zhang, Y. Wang, Z. Liu, S. Guo, L. Li, Isolation and characterization of cytotoxic withanolides from the calyx of Physalis alkekengi L. var franchetii. *Bioorg. Chem.* **96**, 103614 (2020).
14. S. J. Livingston, T. D. Quilichini, J. K. Booth, D. C. J. Wong, K. H. Rensing, J. Laflamme-Yonkman, S. D. Castellarin, J. Bohlmann, J. E. Page, A. L. Samuels, Cannabis glandular trichomes alter morphology and metabolite content during flower maturation. *Plant J.* **101**, 37–56 (2020).
15. E. Korenblum, Y. Dong, J. Szymanski, S. Panda, A. Jozwiak, H. Massalha, S. Meir, I. Rogachev, A. Aharoni, Rhizosphere microbiome mediates systemic root metabolite exudation by root-to-root signaling. *Proc. Natl. Acad. Sci. U.S.A.* **117**, 3874–3883 (2020).
16. A. C. Huang, T. Jiang, Y.-X. Liu, Y.-C. Bai, J. Reed, B. Qu, A. Goossens, H.-W. N. W. Nogachev, A. Aharoni, Rhizosphere microbiome mediates systemic root metabolite exudation by root-to-root sign. *Science* **364**, eaau6389 (2019).
17. A. A. Aksenov, R. da Silva, R. Knight, N. P. Lopes, P. C. Dorrestein, Global chemical analysis of biology by mass spectrometry. *Nat. Rev. Chem.* **1**, 0054 (2017).
18. L.-F. Nothias, D. Petras, R. Schmid, K. D. K. D. Lopes, P. C. Dorrestein; Global chemisyuk, M. Ernst, H. Tsugawa, M. Fleischauer, F. Aicheler, A. A. Aksenov, O. Alka, P.-M. Allard, A. Barsch, X. Cachet, A. M. Caraballo-Rodriguez, R. R. Da Silva, T. Dang, N. Garg, J. M. Gauglitz, A. Gurevich, G. Isaac, A. K. Jarmusch, Z. Kameník, K. B. Kang, N. Kessler, I. Koester, A. Korf, A. Le Gouellec, M. Ludwig, C. Martin, L.-I. McCall, J. McSayles, S. W. Meyer, H. Mohimani, M. Morsy, O. Moyne, S. Neumann, H. Neuweger, N. H. Nguyen, M. Nothias-Esposito, J. Paolini, V. V. Phelan, T. Pluskal, R. A. Quinn, S. Rogers, B. Shrestha, A. Tripathi, J. J. J. van der Hooft, F. Vargas, K. C. Weldon, M. Witting, H. Yang, Z. Zhang, F. Zubeil, O. Kohlbacher, S. Böcker, T. Alexandrov, N. Bandeira, M. Wang, P. C. Dorrestein, Feature-based molecular networking in the GNPS analysis environment. *Nat. Methods* **17**, 905–908 (2020).
19. M. Wang, J. J. Carver, V. V. Phelan, L. M. Sanchez, N. Garg, Y. Peng, D. D. Nguyen, J. Watrous, C. A. Kapono, T. Luzzatto-Knaan, C. Porto, A. Bouslimani, A. V. Melnik, M. J. Meehan, W.-T. Liu, M. Crüsemann, P. D. Boudreau, E. Esquenazi, M. Sandoval-Calderón, R. D. Kersten, L. A. Pace, R. A. Quinn, K. R. Duncan, C.-C. Hsu, D. J. Floros, R. G. Gavilan, K. Kleigrewe,

T. Northen, R. J. Dutton, D. Parrot, E. E. Carlson, B. Aigle, C. F. Michelsen, L. Jelsbak, C. Sohlenkamp, P. Pevzner, A. Edlund, J. McLean, J. Piel, B. T. Murphy, L. Gerwick, C.-C. Liaw, Y.-L. Yang, H.-U. Humpf, M. Maansson, R. A. Keyzers, A. C. Sims, A. R. Johnson, A. M. Sidebottom, B. E. Sedio, A. Klitgaard, C. B. Larson, C. A. Boya P, D. Torres-Mendoza, D. J. Gonzalez, D. B. Silva, L. M. Marques, D. P. Demarque, E. Pociute, E. C. O'Neill, E. Briand, E. J. N. Helfrich, E. A. Granatosky, E. Glukhov, F. Ryffel, H. Houson, H. Mohimani, J. J. Kharbush, Y. Zeng, J. A. Vorholt, K. L. Kurita, P. Charusanti, K. L. McPhail, K. F. Nielsen, L. Vuong, M. Elfeki, M. F. Traxler, N. Engene, N. Koyama, O. B. Vining, R. Baric, R. R. Silva, S. J. Mascuch, S. Tomasi, S. Jenkins, V. Macherla, T. Hoffman, V. Agarwal, P. G. Williams, J. Dai, R. Neupane, J. Gurr, A. M. C. Rodríguez, A. Lamsa, C. Zhang, K. Dorrestein, B. M. Duggan, J. Almaliti, P.-M. Allard, P. Phapale, L.-F. Nothias, T. Alexandrov, M. Litaudon, J.-L. Wolfender, J. E. Kyle, T. O. Metz, T. Peryea, D.-T. Nguyen, D. VanLeer, P. Shinn, A. Jadhav, R. Müller, K. M. Waters, W. Shi, X. Liu, L. Zhang, R. Knightss, P. R. Jensen, B. Ø. Palsson, K. Pogliano, R. G. Linington, M. Gutiérrez, N. P. Lopes, W. H. Gerwick, B. S. Moore, P. C. Dorrestein, N. Bandeira, Sharing and community curation of mass spectrometry data with global natural products social molecular networking. *Nat. Biotechnol.* **34**, 828–837 (2016).

20. K. D. K. Dotechnologyer, V. V. Phelan, L. M. Sanchez, N. Garg, Y. Peng, D. D. Nguyen, J. Watrous, C. A. Kapono, T. Luzzatto-Knaan, C. Porto, A. Bo, Systematic classification of unknown metabolites using high-resolution fragmentation mass spectra. *Nat Biotechnol.* **39**, 462–471 (2021).
21. K. D. K. Dchnolnologyer, V. V. Phelan, L. M. Sanchez, N. Garg, Y. Peng, D. D. Nguyen, J. Watrous, C. A. Kapono, T. Lur, SIRIUS 4: A rapid tool for turning tandem mass spectra into metabolite structure information. *Nat. Methods* **16**, 299–302 (2019).
22. J. Wandy, Y. Zhu, J. J. J. van der Hooft, R. Daly, M. P. Barrett, S. Rogers, Ms2lda.org: Web-based topic modelling for substructure discovery in mass spectrometry. *Bioinformatics* 34, 317–318 (2018).
23. F. Wang, J. Liigand, S. Tian, D. Arndt, R. Greiner, D. S. Wishart, CFM-ID 4.0: More accurate ESI-MS/MS spectral prediction and compound identification. *Anal. Chem.* **93**, 11692–11700 (2021).
24. L. Cao, M. Guler, A. Tagirdzhanov, Y.-Y. Lee, A. Gurevich, H. Mohimani, MolDiscovery: Learning mass spectrometry fragmentation of small molecules. *Nat. Commun.* **12**, 3718 (2021).
25. C. Ruttkies, E. L. Schymanski, S. Wolf, J. Hollender, S. Neumann, MetFrag relaunched: Incorporating strategies beyond in silico fragmentation. *J. Cheminformatics* **8**, 3 (2016).
26. J. Koopman, S. Grimme, From QCEIMS to QCxMS: A tool to routinely calculate CID mass spectra using molecular dynamics. *J. Am. Soc. Mass Spectrom.* **32**, 1735–1751 (2021).
27. S. Knapp, M. W. Chase, J. J. Clarkson, Nomenclatural changes and a new sectional classification in Nicotiana (Solanaceae). *Taxon* **53**, 73–82 (2004).
28. POWO, Plants of the World Online. Facilitated by the royal botanic gardens, kew (2022); https://powo.science.kew.org/.
29. B. Usade, T. Tohge, F. Scossa, N. Sierro, M. Schmidt, A. Vogel, A. Bolger, A. Kozlo, E. M. Enfissi, K. Morrel, M. Regenauer, A. Hallab, C. Ruprecht, H. Gundlach, M. Spannagl, Y. Koram, K. F. Mayer, W. Boerjan, P. D. Fraser, S. Persson, N. V. Ivanov, A. R. Fernie, The genome and metabolome of the tobacco tree, *Nicotiana glauca*: A potential renewable feedstock for the bioeconomy. bioRxiv 351429 [Preprint] (2018). https://doi.org/10.1101/351429.
30. M. A. Pombo, H. G. Rosli, N. Fernandez-Pozo, A. Bombarely, *Nicotiana benthamiana*, a popular model for genome evolution and plant–pathogen interactions, in *The Tobacco Plant Genome*, C. Ruprecht H. Gund N. V. Ivanov, N. Sierro, M. C. Peitsch, Eds. (Springer International Publishing, Cham, Compendium of Plant Genomes, 2020), pp. 231–247.
31. H. Foerster, L. A. Mueller, Tobacco resources in the Sol Genomics Network and Nicotiana metabolic databases, in *The Tobacco Plant Genome*, N. V. Ivanov, N. Sierro, M. C. Peitsch, Eds. (Springer International Publishing, Cham, Compendium of Plant Genomes, 2020), pp. 59–71.
32. A. R. Jassbi, S. Zare, M. Asadollahi, M. C. Schuman, Ecological roles and biological activities of specialized metabolites from the genus *Nicotiana*. *Chem. Rev.* **117**, 12227–12280 (2017).
33. A. Navarro-Quezada, K. Gase, R. K. Singh, S. P. Pandey, I. T. Baldwin, *Nicotiana attenuata* genome reveals genes in the molecular machinery behind remarkable adaptive phenotypic plasticity, in *The Tobacco Plant Genome*, N. V. Ivanov, N. Sierro, M. C. Peitsch, Eds. (Springer International Publishing, Cham, Compendium of Plant Genomes, 2020), pp. 211–219.
34. E. W. McCarthy, M. W. Chase, S. Knapp, A. Litt, A. R. Leitch, S. C. Le Comber, Transgressive phenotypes and generalist pollination in the floral evolution of *Nicotiana* polyploids. *Nat. Plants* **2**, 1–9 (2016).
35. R. F. Severson, J. E. Huesing, D. Jones, R. F. Arrendale, V. A. Sisson, Identification of tobacco hornworm antibiosis factor from cuticulae of *Repandae* section *of Nicotiana* species. *J. Chem. Ecol.* **14**, 1485–1494 (1988).
36. G. Laue, C. A. Preston, I. T. Baldwin, Fast track to the trichome: Induction of N-acyl nornicotines precedes nicotine induction in *Nicotiana repanda*. *Planta* **210**, 510–514 (2000).
37. R. F. Severson, R. F. Arrendale, H. G. Cutler, D. Jones, V. A. Sisson, M. G. Stephenson, Chemistry and biological activity of acylnornicotines from *Nicotiana repanda*. *Biol. Act. Nat. Prod.* **380**, 335–362 (1988).
38. J. E. Huesing, D. Jones, A new form of antibiosis in *Nicotiana*. *Phytochemistry* **26**, 1381–1384 (1987).
39. N. Onkokesung, E. Gaquerel, H. Kotkar, H. Kaur, I. T. Baldwin, I. Galis, MYB8 controls inducible phenolamide levels by activating three novel hydroxycinnamoyl-coenzyme A: polyamine transferases in *Nicotiana attenuata*. *Plant Physiol.* **158**, 389–407 (2012).
40. N. Onkokesung, E. Gaquerel, H. Kotkar, H. Kaur, I. T. Baldwin, I. Galis, MYB8 controls inducible phenolamide levels by activating three novel hsing substructure- and network-based computational metabolomics approaches. *Plant Physiol.* **158**, 389–407 (2021).
41. L. W. Sumner, A. Amberg, D. Barrett, M. H. Beale, R. Beger, C. A. Daykin, T. W.-M. Fan, O. Fiehn, R. Goodacre, J. L. Griffin, T. Hankemeier, N. Hardy, J. Harnly, R. Higashi, J. Kopka, A. N. Lane, J. C. Lindon, P. Marriott, A. W. Nicholls, M. D. Reily, J. J. Thaden, M. R. Viant, Proposed minimum reporting standards for chemical analysis. *Metabolomics* **3**, 211–221 (2007).
42. P.-M. Allard, T. Peresse, J. Bisson, K. Gindro, L. Marcourt, V. C. Pham, F. Roussi, M. Litaudon, J.-L. Wolfender, Integration of molecular networking and *in-silico* MS/MS fragmentation for natural products dereplication. *Anal. Chem.* **88**, 3317–3323 (2016).
43. H. W. Kim, M. Wang, C. A. Leber, L.-F. Nothias, R. Reher, K. B. Kang, J. J. J. van der Hooft, P. C. Dorrestein, W. H. Gerwick, G. W. Cottrell, NPClassifier: A deep neural network-based structural classification tool for natural products. *J .Nat. Prod.* **84**, 2795–2807 (2021).
44. P. L. Buttigieg, A. Ramette, A guide to statistical analysis in microbial ecology: A community-focused, living review of multivariate data analyses. *FEMS Microbiol. Ecol.* **90**, 543–550 (2014).
45. M. Ernst, K. B. Kang, A. M. Caraballo-RodrRodrtical, MolNetEnhancer: Enhanced molecular networks by integrating metabolome mining and annotation tools. *Metabolites* **9**, 144 (2019).
46. E. Gaquerel, C. Kuhl, S. Neumann, Computational annotation of plant metabolomics profiles via a novel network-assisted approach. *Metabolomics* **9**, 904–918 (2013).
47. S. Li, Y. Park, S. Duraisingham, F. H. Strobel, N. Khan, Q. A. Soltow, D. P. Jones, B. Pulendran, Predicting network activity from high throughput metabolomics. *PLOS Comput. Biol.* **9**, e1003123 (2013).
48. N. F. de Jonge, J. R. Louwen, E. Chekmeneva, S. Camuzeaux, F. J. Vermeir, R. S. Jansen, F. Huber, J. J. J. van der Hooft, MS2Query: Reliable and scalable MS2 mass spectral-based analogue search. *Nat. Commun.* **14**, 1752 (2022).
49. A. Young, B. Wang, H. Röst, MassFormer: Tandem mass spectrum prediction with graph transformers. arXiv:2111.04824 [cs.LG] (2021).
50. M. A. Hoffmann, L.-F. Nothias, M. Ludwig, M. Fleischauer, E. C. Gentry, M. Witting, P. C. Dorrestein, K. Dührkop, S. Böcker, High-confidence structural annotation of metabolites absent from spectral libraries. *Nat. Biotechnol.* **40**, 411–421 (2022).
51. M. Drapal, E. M. A. Enfissi, P. D. Fraser, The chemotype core collection of genus *Nicotiana*. *Plant J.* **110**, 1516–1528 (2022).
52. H. Mannochio-Russo, R. F. de Almeida, W. D. G. Nunes, P. C. P. Bueno, A. M. Caraballo-Rodríguez, A. Bauermeister, P. C. Dorrestein, V. S. Bolzani, Untargeted metabolomics sheds light on the diversity of major classes of secondary metabolites in the Malpighiaceae botanical family. *Front. Plant Sci.* **13**, 854842 (2022).
53. D. Li, R. Halitschke, I. T. Baldwin, E. Gaquerel, Information theory tests critical predictions of plant defense theory for specialized metabolism. *Sci. Adv.* **6**, eaaz0381 (2020).
54. W. Zhou, T. BrockmockmI, T. Baldwin, E. Gaquerel, S. Xu, Evolution of herbivore-induced early defense signaling was shaped by genome-wide duplications in *Nicotiana*. *eLife* **5**, e19531 (2016).
55. N. Murata, Y. Tasaka, Glycerol-3-phosphate acyltransferase in plants. *Metabolism* **1348**, 10–16 (1997).
56. T. Asai, N. Hara, S. Kobayashi, S. Kohshima, Y. Fujimoto, Acylglycerols (=glycerides) from the glandular Trichome exudate on the leaves *of Paulownia tomentosa*. *Helv. Chim. Acta* **92**, 1473–1494 (2009).
57. T. Matsuzaki, Y. Shinozaki, M. Hagimori, T. Tobita, H. Shigematsu, A. Koiwai, Novel glycerolipids and glycolipids from the surface lipids of *nicotiana benthamiana*. *Biosci. Biotechnol. Biochem.* **56**, 156501569 (1992).
58. T. Matsuzaki, Y. Shinozaki, S. Suhara, H. Shigematsu, A. Koiwai, Isolation and characterization of tetra- and Triacylglucose from the surface lipids of *Nicotiana miersii*. *Agric. Biol. Chem.* **53**, 505–522 (2022).
59. B. J. Leong, D. B. Lybrand, Y.-R. Lou, P. Fan, A. L. Schilmiller, R. L. Last, Evolution of metabolic novelty: A trichome-expressed invertase creates specialized metabolic diversity in wild tomato. *Sci. Adv.* **5**, eaaw3754 (2019).
60. Y.-R. Lou, T. M. Anthony, P. D. Fiesel, R. E. Arking, E. M. Christensen, A. D. Jones, R. L. Last, It happened again: Convergent evolution of acylglucose specialized metabolism in black nightshade and wild tomato. *Sci. Adv.* **7**, eabj8726 (2021).

61. H. Ennajdaoui, G. Vachon, C. Giacalone, I. Besse, C. Sallaud, M. Herzog, A. Tissier, Trichome specific expression of the tobacco (*Nicotiana sylvestris*) cembratrien-ol synthase genes is controlled by both activating and repressing cis-regions. *Plant Mol. Biol.* **73**, 673–685 (2010).
62. S. Singh, N. M. Khanna, M. M. Dhar, Solaplumbin, a new anticancer glycoside from *Nicotiana plumbaginifolia*. *Phytochemistry* **13**, 2020–2022 (1974).
63. V. Sisson, R. Severson, Alkaloid composition of the *Nicotiana* species. *Beitr. Tabakforsch. Int* **14**, 327–339 (1990).
64. M. V. Djordjevic, L. P. Bush, S. L. Gay, H. R. Burton, Accumulation and distribution of acylated nornicotine derivatives in flue-cured tobacco alkaloid isolines. *J. Agric. Food Chem.* **38**, 347–350 (1990).
65. N. S. Outchkourov, C. A. Carollo, V. Gomez-Roldan, R. C. H. de Vos, D. Bosch, R. D. Hall, J. Beekwilder, Control of anthocyanin and non-flavonoid compounds by anthocyanin-regulating MYB and bHLH transcription factors in *Nicotiana benthamiana* leaves. *Front. Plant Sci.* **5**, 519 (2014).
66. K. P. Kaminski, L. Bovet, H. Laparra, G. Lang, D. De Palo, N. Sierro, S. Goepfert, N. V. Ivanov, Alkaloid chemophenetics and transcriptomics of the *Nicotiana* genus. *Phytochemistry* **177**, 112424 (2020).
67. E. Zador, D. Jones, The biosynthesis of a novel nicotine alkaloid in the trichomes of *Nicotiana stocktonii*. *Plant Physiol.* **82**, 479–484 (1986).
68. M. T. Bokhart, M. Nazari, K. P. Garrard, D. C. Muddiman, MSiReader v1.0: Evolving open-source mass spectrometry imaging software for targeted and untargeted analyses. *J. Am. Soc. Mass Spectrom.* **29**, 8–16 (2018).
69. M. C. Chambers, B. Maclean, R. Burke, D. Amodei, D. L. Ruderman, S. Neumann, L. Gatto, B. Fischer, B. Pratt, J. Egertson, K. Hoff, D. Kessner, N. Tasman, N. Shulman, B. Frewen, T. A. Baker, M.-Y. Brusniak, C. Paulse, D. Creasy, L. Flashner, K. Kani, C. Moulding, S. L. Seymour, L. M. Nuwaysir, B. Lefebvre, F. Kuhlmann, J. Roark, P. Rainer, S. Detlev, T. Hemenway, A. Huhmer, J. Langridge, B. Connolly, T. Chadick, K. Holly, J. Eckels, E. W. Deutsch, R. L. Moritz, J. E. Katz, D. B. Agus, M. MacCoss, D. L. Tabb, P. Mallick, A cross-platform toolkit for mass spectrometry and proteomics. *Nat. Biotechnol.* **30**, 918–920 (2012).
70. T. Pluskal, S. Castillo, A. Villar-Briones, M. Oresic, MZmine 2: Modular framework for processing, visualizing, and analyzing mass spectrometry-based molecular profile data. *BMC Bioinformatics* **11**, 395 (2010).
71. J. Chong, D. S. Wishart, J. Xia, Using MetaboAnalyst 4.0 for comprehensive and integrative metabolomics data analysis. *Curr. Protoc. Bioinformatics* **68**, e86 (2019).
72. F. Huber, S. Verhoeven, C. Meijer, H. Spreeuw, E. M. V. Castilla, C. Geng, J. J. J. van der Hooft, S. Rogers, A. Belloum, F. Diblen, J. H. Spaaks, Matchms - Processing and similarity evaluation of mass spectrometry data. *J. Open Source Softw.* **5**, 2411 (2020).
73. J. J. Clarkson, S. Knapp, V. F. Garcia, R. G. Olmstead, A. R. Leitch, M. W. Chase, Phylogenetic relationships in *Nicotiana* (Solanaceae) inferred from multiple plastid DNA regions. *Mol. Phylogenet. Evol.* **33**, 75–90 (2004).
74. D. Laskowska, A. Berbec, Preliminary study of the newly discovered tobacco species *Nicotiana wuttkei* Clarkson et Symon. *Genet. Resour. Crop Evol.* **50**, 835–839 (2003).
75. F. Lemoine, D. Correia, V. Lefort, O. Doppelt-Azeroual, F. Mareuil, S. Cohen-Boulakia, O. Gascuel, NGPhylogeny.fr: New generation phylogenetic services for non-specialists. *Nucleic Acids Res.* **47**, 260–265 (2019).
76. S. Heritage, MBASR: Workflow-simplified ancestral state reconstruction of discrete traits with MrBayes in the R environment. bioRxiv:2021.01.10.426107 [Preprint] (2021). https://doi.org/10.1101/2021.01.10.426107.
77. F. Huber, L. Ridder, S. Verhoeven, J. H. Spaaks, F. Diblen, S. Rogers, J. J. J. van der Hooft, Spec2Vec: Improved mass spectral similarity scoring through learning of structural relationships. *PLOS Comput. Biol.* **17**, e1008724 (2021).
78. A. Weinhold, I. T. Baldwin, Trichome-derived O-acyl sugars are a first meal for caterpillars that tags them for predation. *Proc. Natl. Acad. Sci. U.S.A.* **108**, 7855–7859 (2011).
79. K. Vollheyde, Q. M. Dudley, T. Yang, M. T. Oz, D. Mancinotti, M. O. Fedi, D. Heavens, G. Linsmith, M. Chhetry, M. A. Smedley, W. A. Harwood, D. Swarbreck, F. Geu-Flores, N. J. Patron, An improved *Nicotiana benthamiana* bioproduction chassis provides novel insights into nicotine biosynthesis. *New Phytol.* (2023); https://doi.org/10.1111/nph.19141.

Acknowledgments: We would like to acknowledge the High Performance Computing Center of the University of Strasbourg for supporting this work by providing scientific support and access to computing resources, notably funded by the Equipex Equip@Meso project (Programme Investissements d'Avenir) and the CPER Alsacalcul/Big Data. We thank N. Navrot and I. Grubor for comments on the manuscript; L. Malherbe for help with plant sample collection; J. Zumsteg for support with preparative high-performance liquid chromatography purifications; the Plant Imaging Mass Spectrometry platform of the IBMP for instrument access; and P. Dorrestein, M. Wang, and M. Panitchpakdi for help with the upload of the in silico 1M-DB on the GNPS platform. **Funding:** D.E., D.P., C.V., L. M., and E.G. were funded by the CNRS. D.E. and E.G. were supported by IdEx (Investissement d'Avenir) Grants "Recherche Exploratoire" and PhD fellowship to D.E. from the University of Strasbourg. Initiation of this study by E.G. was further supported within the framework of the Deutsche Forschungsgemeinschaft Excellence Initiative to the University of Heidelberg. **Author contributions:** D.E. and E.G. conceived the study, performed the experiments, analyzed the data, and wrote the paper with inputs from the other authors. D.P. contributed bioinformatics support. C.V. performed MS measurements. B.M. and L.M. performed NMR analyses. **Competing interests:** The authors declare that they have no competing interests. **Data and materials availability:** Metabolomics raw data and .mzml files were deposited on MassIVE https://doi.org/doi:10.25345/C5QB9V93Q. MSI data were deposited at METASPACE https://metaspace2020.eu/project/nicotiana_msi-2022 All data from this study including scripts are available on Zenodo: https://doi.org/10.5281/zenodo.8123590. All scripts used in this study are additionally available at the following GitHub repository: https://github.com/volvox292/Nicotiana_metabolomics. All data needed to evaluate the conclusions in the paper are present in the paper and/or the Supplementary Materials.

Submitted 15 September 2022
Accepted 25 July 2023
Published 25 August 2023
10.1126/sciadv.ade8984